(NASA-CR-170128) SUPPORT OF RESEARCH IN X-RAY ASTRONOMY Final Technical Report (Pennsylvania State Univ.) 104 p
HC A06/MF A01 CSCL 03A

N83-22073

Unclas
H2/89 03231

Final Technical Report for NASA Grant NAGW-108

"Support of Research in X-ray Astronomy"

18 February 1983

Gordon Garmire
(814) 865-1117
Principal Investigator
Department of Astronomy
Pennsylvania State University
University Park, PA 16802
(814) 865-0418

L. J. Kaluzienski
NASA Technical Officer
Code SC-7
(202) 755-8493

1.0 Introduction

The research activities supported by this contract include the evaluation of CCD detectors for x-ray astronomy applications, contributions to the development of an imaging gas scintillation proportional counter, the evaluation of certain metal oxide crystals as potential radiation detectors, optical observations and searches for x-ray sources discovered by the HEAO-1 A2 experiment, and theoretical modeling of non equilibrium ionization structure of supernova remnants.

2.0 Detector Development

2.1 Evaluation of CCD detectors for x-ray astronomy

A program of CCD evaluation for x-ray astronomy was initiated under a President's Fund at CalTech (PF173) and the Jet Propulsion Laboratory in Pasadena, California. The purpose of the investigation was to irradiate existing CCD devices being used in optical wavelengths with x-rays to determine their performance characteristics as x-ray detectors. The funding was quite limited and only allowed for the testing of a few existing devices. The initial tests were not very encouraging, but did show that the optical CCD detectors were sensitive to x-rays. The energy resolution was very poor and the efficiency was low. In order to continue this work, we proposed to use some grant money NAGW-108 as well as requesting an additional President's Fund for one more year of effort. The extra support was still not adequate to produce CCD's more optimally designed for x-ray detectors, but did permit more testing and some electronic modifications in the readout processing.

One immediate benefit to both the Space Telescope Project and the Galileo Project was that the x-ray data provided a good evaluation signal (which were hard to obtain using visible light) to determine parameters for the optical chips. This situation occured because the x-ray interaction generated a precise amount of charge in the CCD which could be used to evaluate charge transfer characteristics in the silicon material of the chip.

Improvements in signal processing of the charge transfer in the three phase clocked CCD's resulted in a much improved performance. These results were presented at GSFC on October 6, 1981 (Riegler et al 1981). A new virtual phase device was evaluated for this report as well. All CCD's were produced by Texas Instruments since they were the ones being used for Space telescope and the Galileo Project.

Further testing has continued following the above report. Considerable improvements have been made as reported by Stern et al 1983. At this time the energy resolution and detection efficiency are close to the theoretical values for silicon. It is likely, that with the production of x-ray optimized CCD's which are now being fabricated at Texas Instruments, the resolution which is set by the energy required to produce an ion-electron pair and the Fano factor for silicon will be realized.

A proposal was submitted on the basis of the above results and has been funded by NASA for making X-ray optimized devices and to fly one of these detectors on a sounding rocket to evaluate background levels and detector performance at the focus of a Wolter Type I x-ray telescope.

3.0 Gas Scintillation Proportional Counter Observation of M87

An Imaging Gas Scintillation Proportional Counter (IGSPC) was developed by the Los Alamos National Laboratory's Astrophysics branch under the direction of Dr. Doyle Evans. Dr. Richard Blake together with Dr. David Anderson undertook the detector development at LANL. A 15" diameter Wolter Type I mirror assembly (see Tuohy et al 1979) was combined with the IGSPC to form an imaging instrument with superior energy resolution and high detection efficiency. The energy resolution achieved for the flight instrument was 7.9% at 5.9 keV, with a position resolution of 1mm at this energy. Pulse rise time information was available for background rejection. The following sections describe the preliminary results from the rocket flight which took place on 21 June 1982.

3.1 Scientific Rationale and Choice of Target.

The IPC (Imaging Proportional Counter) flown on the Einstein Observatory prosessed good detection efficiency over the 0.2-40 keV energy band, moderate spatial resolution $\sim$1 mm, poor energy resolution, 120% at 1.5 keV, and some background rejection efficiency $\sim$50% of the cosmic rays. In order to improve on this capability for future x-ray astronomy missions, better position resolution, energy resolution and background rejection present themselves as possible areas for investigation. The gas scintillation detector had been developed over the previous decade, to where the possibility for a substantial gain in energy resolution could be made. The positioning of an event, however, posed a more difficult problem. Optical systems could be used to locate the light pulse in the scintillation chamber either as in an Anger Camera used with crystal scintillators, or by imaging of the scintillation light on an optical imaging detector.

A clever solution to this problem was discovered by David Anderson, at

LANL who showed that by adding a small amount of TMAE to a proportional counter gas that it could be rendered sensitive to the UV light produced by scintillation in Xenon gas. This discovery made it possible to combine the superior energy resolution of the gas scintillation counter with the position resolution of the imaging proportional counter. Since this technique preserved the inherent good timing characteristics of the proportional counter, the rise time of the light pulse could be measured at the same time as the position and energy thereby providing the possibility of improved background rejection.

The Einstein Observatory has obtained extensive observations of the brighter supernova remnants and clusters of galaxies, both classes of targets which are the only ones available for detailed observations from sounding rockets. In order to obtain improved information over the Einstein results, it is necessary to make observations with either improved spectral and/or spatial characteristics. The IGSPC offers such a possibility in that the IGSPC has the spatial resolution of the IPC and the energy resolution of the SSS, thereby offering in one observation the capability of both instruments on the Einstein Observatory. The two brightest targets with adequate spatial extent and appropriately emitting spectral properties matching the combined telescope-detector response are Pup A and M87. The latter source is a little low in intensity, but not so low as to be severly photon statistics limited.

3.2 The Instrument Performance and Initial Results

The IGSPC was flown with the 15" Wolter Type I telescope from WSMR on 21 June 1982 using a boasted Black Brant (27.068 AH). The flight was completely successful, in that M87 was acquired for the entire flight of some 250 seconds above 130 km altitude. The aspect camera showed that M87 was held to witnin about one resolution element during the entire exposure, and positioned very near the center of the detector.

A calibration source illuminated the detector with $A\ell K_\alpha$ x-rays both at the beginning and end of the flight. The pulse height distribution is shown in Figure 2-1, indicating an energy resolution of about 22%, a factor of 1.5 better than a typical proportional counter resolution such as obtained on HEAO-1.

The rise time distribution of events produced by the $A\ell K_\alpha$ source provides a measure of the x-ray induced time spread. The cosmic ray and gamma ray induced events come from the region outside of the telescope field of view. Their distribution of rise times is much broader, especially toward longer rise time. The rejection efficiency for this particular counter is about 70% at 1.5 keV. The x-ray rise time distribution was not found to be energy dependent between 1.5 and 5.9 keV.

The position resolution of the detector has been measured in the laboratory as a function of energy. At 5.9 keV the resolution is about 1mm. At $A\ell K_\alpha$ the resolution degrades to 2mm, becoming progressively worse as the energy is lowered. At this level of position resolution, the angular resolution of the experiment is dominated by the detector and not the mirrors which have about a 2 arc minute resolution (note that 1mm corresponds to 1.7 arc minutes in the focal plane).

The rocket flight only recorded about 600 x-ray events from M87. This is less than anticipated which was mostly caused by a high threshold on the low energy discriminator to reject noise in the emplifiers used on the cathode wires for position sensing.

About one third of the events originate from the cluster core where possible heavy element sedimentation and rapid cooling of the hot gas may be occuring. Detailed modeling and fitting of the data has not been completed at this time. Given the low statistical quality of the data, it is unlikely that no more than upper limits will be set to evolution in the cluster core region.

Figure Captions

Figure 1

In flight calibration of the IGSPC prior to and following the M87 observation. The energy resolution is about 22%, FW HM.

Figure 2

The rise time distribution of $A\ell k_{\alpha}$ events compared to the cosmic ray background.

Figure 3

The spectrum of the core, inner 4 arc minutes, and the halo of M87. Spectral modelling of this data has not been completed.

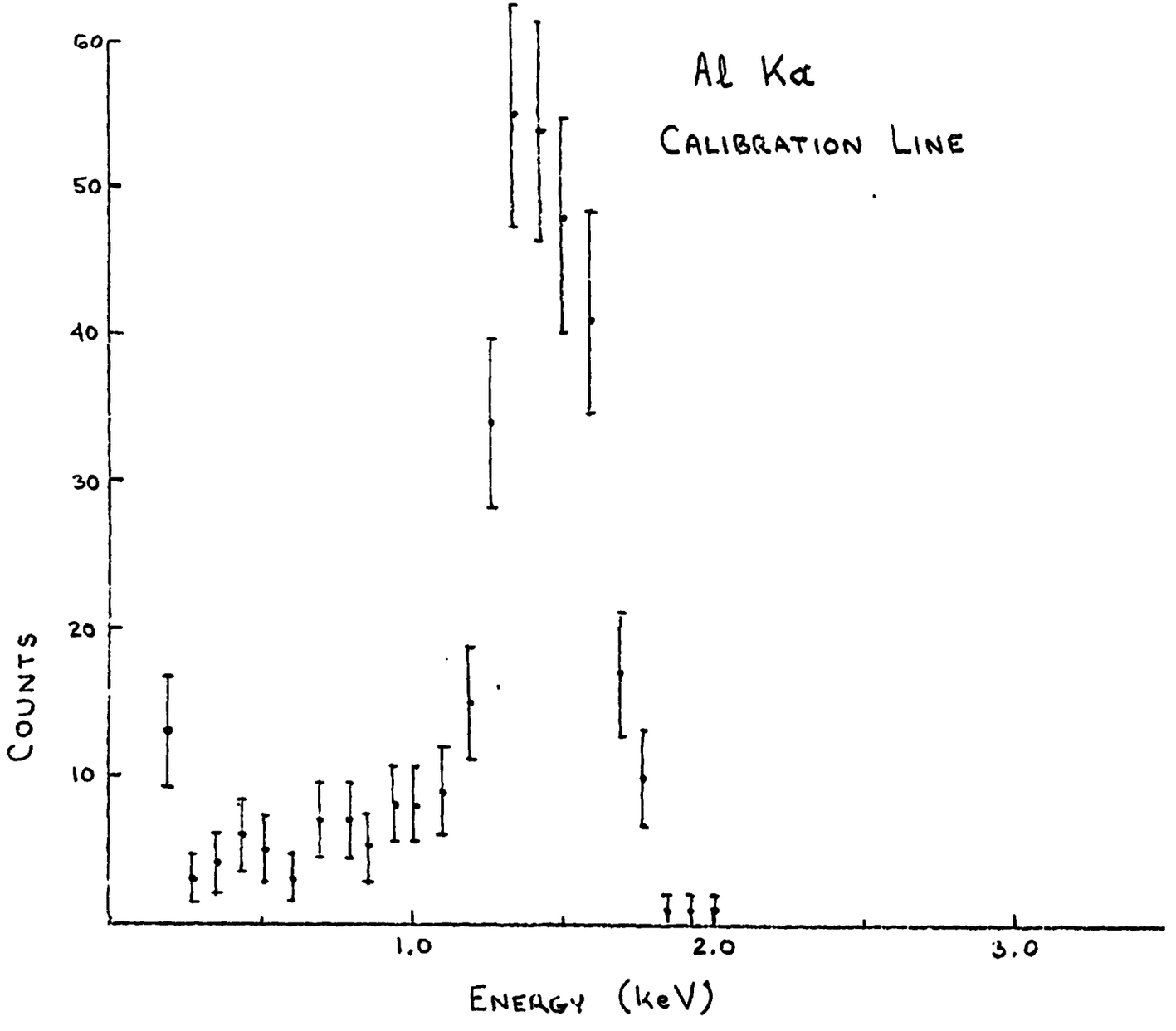

JAN

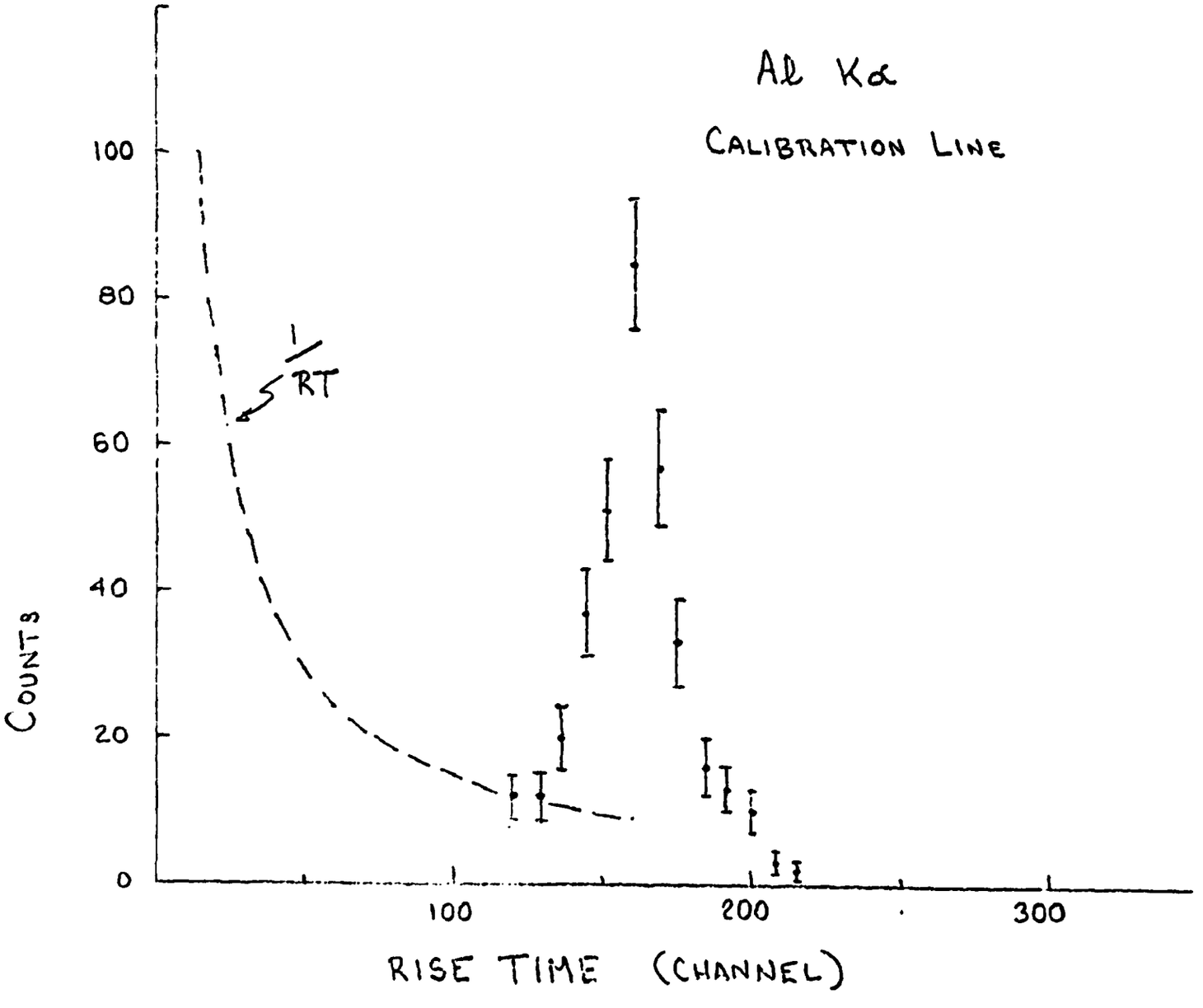

JM
3/1/

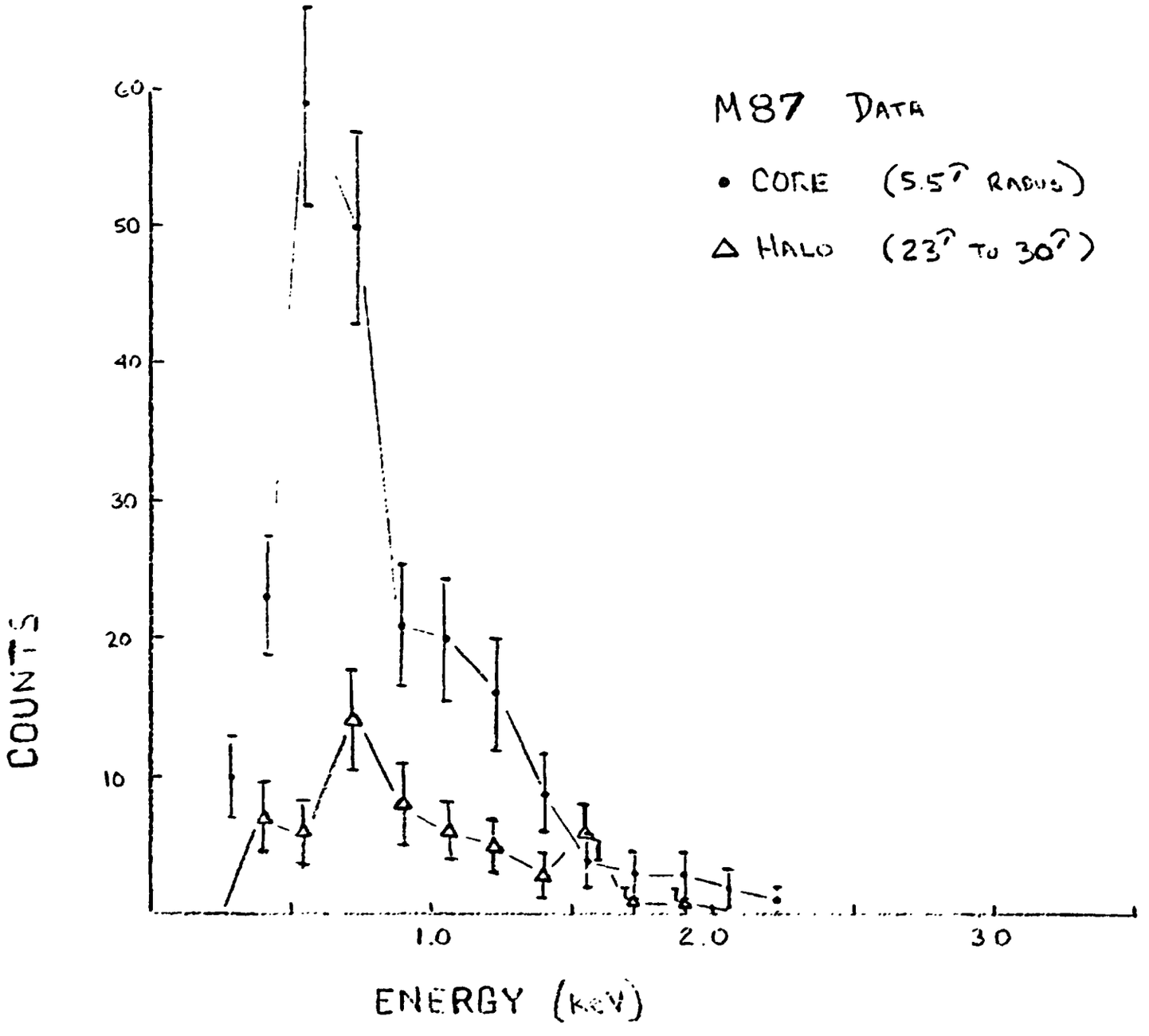

JAN
4/1/

4.0 Non-Equilibrium X-ray Emission from Young Supernova Remnants

Young Supernova Remnants (SNR) emit strongly in the x-ray band of the spectrum. Numerous lines from a variety of elements have been observed in their emission spectrum (Winkler et al 1981, Becker et al 1980). Because these emission lines are generated in a hot dynamic medium which is undergoing rapid expansion, the emission lines are produced in a non equilibrium condition (Moore and Garmire, 1976, Itoh, 1978). Since young SNR's still contain a substantial fraction of the ejected material of the parent star relative to swept up interstellar gas (ISM), it is of great scientific interest to attempt to determine the actual abundance of elements in the SNR with the goal of determining something about the final stages of stellar evolution and the enrichment of the interstellar medium via supernova explosions. Detailed modeling is essential, since the plasma is far from collisional equilibrium. The following calculations are only a first step in this investigation since the detailed nature of the initial conditions for any given SNR such as the density distribution of the local ISM and the initial blast energies are never known with precision and certainly vary from remnant to remnant. For a detailed discussion of the hydrodynamics and calculational methods refer to the CalTech Thesis by the same title written by John Nugent Jr.

4.1 Outline of the Model

The hydrodynamics are calculated assuming a spherical supernova explosion of energy, E_o, which expands into a uniform ISM with particle density, n_o. The energy is assumed initially to be almost completely contained in the ballistic motions of the ejecta. The flow of the gas, except at shock fronts, is assumed to be adiabatic, so heat conduction and radiative cooling are neglected. An explicit set of finite-element equations representing the Lagrangian equations were used in the calculation. These equations, which were taken from Richtmyer

and Morton (1967), included the artificial viscosity term, which acts as a dissipative mechanism at shock fronts. The number of spherical shells used for the ejecta was 13 and the number for the shocked ISM varied from 12 to 24. The number of shells was constrained by CPU memory and time considerations. Discontinuities in density at the ejecta/ISM interface and at the jump at the main forward shock were smoothed slightly because of the finite number of shells resulting in some minor underestimate of the emission from these regions relative to the rest of the remnant.

Thus, given E_o, n_o, and the mass of the ejected material, M_e, the mean temperature, T_m, and the electron density, n_e, can be calculated as a function of time and radius. The calculation of the electron temperature, T_e, depends on the question of non-Coulomb processes at the shock front. Two extreme cases will be examined. The first is to assume that the electrons come across the shock front "cold" and are subsequently heated by Coulomb-like collisions with the ions. The second is to assume that some mechanism at the shock front y brings the electrons and ions into thermal equilibrium. Under those conditions $T_e = T_i = T_m$.

Once the history of T_e and n_e in a given shell is known, the fractional population of ionic state with charge, z of an element with nuclear Z, can be found by integrating

$$\frac{1}{n_e}\frac{dX_{Z,z}}{dt} = i_{Z,z-1} X_{Z,z-1} - (i_{Z,z}+r_{Z,z})X_{Z,z} + r_{Z,z+1} X_{Z,z+1}$$

where $X_{Z,z}$ is the fractional population, $n_e i_{Z,z}$ is the rate for an atom with nuclear Z in ionic state z to ionize to state z + 1 via electron collisions, and $n_e r_{Z,z}$ is the rate for an atom with nuclear charge Z and ionic state z to recombine with an electron to form ionic state z-1. The fractional concentration is defined such that

$$\sum_{z=1}^{Z+1} X_{Z,z} = 1.$$

The set of values $\{X_{Z,1}, X_{Z,2},\ldots,X_{Z,Z+1}\}$ shall hereafter be referred to as the ionization structure of the element with nuclear charge Z.

Some pre-ionization must occur in front of the shock for a collisionless shock front in relatively low states of ionization. Hydrogen and helium are assumed to be initially stripped. The rest of the elements considered and their given initial state are: C^{+4}, N^{+5}, Ne^{+5}, Mg^{+5}, Si^{+5}, S^{+6}, Ar^{+6}, Ca^{+6}, Fe^{+6}, and Ni^{+6}. Because of the relatively large ionization rates that still occur at these early stages of ionization, the transient effects caused by this ad hoc choice of initial conditions should be eliminated in $\sim$ 10-20 years.

The final step is to use the electron temperature, electron density, and ionization structure to calculate the spectrum from each element in each shell. A modified version of the Raymond and Smith plasma code (1977) is used. The collisional excitation rates for He-like ions were changed to those calculated by Pradhan, Norcross, and Hummer (1981), which, unlike earlier calculations included effects of autoionizing resonances. Also, a number of processes that produce Kα photons from iso-sequences with lower ionic charge than He-like ions have been added. The original Raymond and Smith code only considers innershell excitation for Li-like, Be-like, and occasionally B-like ions. This is sufficient in a CIE plasma because if the temperature is high enough to excite Kα emission from lower iso-sequences (i.e. if $T_e \gtrsim E_{K\alpha}$) then the iso-sequences below B-like are in very low concentrations. This is not necessarily the case when the plasma is in non-ionization equilibrium (NIE) especially for the higher Z elements. For the densities and time scales applicable in the SNR problem, we felt it was adequate to augment the Kα processes only for Ar, Ca, Fe, and Ni. Innershell excitation to the L-shell has been added, then, for all iso-sequences between Li-like and F-like ions of these elements. In addition, for these elements, innershell

ionization for all iso-sequences below Li-like and the process of producing K shell vacancies via di-electronic recombination has been added for iso-sequences between Li-like and O-like ions. Both these processes result in Kα emission. Excitation rates, branching ratios, and resulting photon energies for these innershell processes are taken from Gronenschild (1979 and references within (e.g. Mewe, Schrijver, and Sylwester (1980)).

Parameterization of the model

The input parameters to the model and the units we will always use are the initial blast energy, E_o (units of 10^{51} ergs), the density of the interstellar medium around the progenitor star, n_o (units of 1 cm^{-3}), the amount of ejected mass from the progenitor star, M_e (units of $M_\odot$), the age of the remnant, t_3 (units of 1000 years), the abundance, relative to hydrogen, of elements in the ejecta (normalized to the measured solar value), the abundance, relative to hydrogen, of elements in the ISM (normalized to the measured solar value), and the distance to the remnant, D (units of kpc). We also will define a "filling factor", f, that gives the fraction of the solid angle of the remnant that is filled with shocked plasma. Finally, we also fit for the amount of neutral hydrogen, N_H (units of 10^{22} cm^2) intervening between the remnant and the earth. This latter quantity parameterizes the energy dependent attenuation along the line of sight due to photoelectric absorption and scattering. The Fireman model (1974) was used for this calculation.

Since the calculation of the spectrum for a choice of E_o, n_o, M_e, and the age, t_3, takes a relatively large amount of computer time, it is necessary, in order to do spectral fitting, to interpolate from a grid. By exploiting a scaling law, we need only to store the results on a three dimensional grid. As discussed by a number of authors a given set of parameters E_o, n_o, M_e, t_3, and D does not produce a unique spectrum (e.g. Mansfield and Salpeter, 1977). An

infinite set of those five parameters can be found that produce the same spectrum for the same abundance set. This degeneracy can be discussed in terms of a scaling parameter defined as

$$\alpha = \left(\frac{E_o}{n_o}\right)^{1/3}$$

as well as a number of "reduced" parameters:

$$\eta = (E_o n_o^2)^{1/3} = \alpha^{-2} E_o = \alpha n_o,$$

$$\beta = \frac{M_e}{E_o} = \eta^{-1}\alpha^{-2} M_e ,$$

and

$$\tau = \left(\frac{n_o}{E_o}\right)^{1/3} t_3 = \alpha^{-1} t_3 .$$

A fourth reduced parameter is the reduced emission volume, C_{ev} which is defined as

$$C_{ev} \equiv \frac{\int n_e^2 dV}{4\pi D^2}$$

and can be expressed as

$$C_{ev} = \frac{\alpha T_{ev}' f}{4\pi D^2}$$

where T_{ev}' is a function of η,β, and τ and is defined as

$$T_{ev}'(\eta,\beta,\tau) \equiv \alpha^{-1} \int n_e^2 dV .$$

We will quote C_{ev} in units of 10^{13} cm^{-5}.

These four reduced parameter along the N_H and the abundance sets of the ejecta and ISM form the parameter space searched when fitting spectra. Once a point in this reduced space is determined to be the best fit, the next problem is to invert from the fitted parameters (η,β,τ, and C_{ev}) to the physical supernova parameters (E_o,n_o,M_e,t_3,f, and D). So far we have shown four equations for six unknowns. A fifth equation can be added that relates the angular radius of the shock front, θ, a measured quantity, to R_s', which is defined by

$$R_s'(\beta,\tau) \equiv \alpha^{-1} R_s$$

where R_s is the true size of the shock radius and R_s' is a function of β and τ. Since $\theta D = R_s$, we can write

$$R_s' = \alpha^{-1}\theta D \ .$$

This still leaves the system of equations underdetermined by one variable. Our approach will be to assume f to be unity and show how the deduced parameters scale with f. Taking that approach, the equation for C_{ev} and the equation for R_s' can be combined to yield the following expression for α:

$$\alpha = \frac{T_{ev}'(\eta,\beta,\tau)\theta^2}{4\pi R_s'^2(\beta,\tau)C_{ev}} f$$

With α, the input parameters are given by

$$E_o = \alpha^2\eta \quad M_e = \alpha^2\eta\beta \quad t_3 = \alpha\tau \quad n_o = \alpha^{-1}\eta$$

and the distance is given by

$$D = \frac{R_s'\alpha}{\theta} \ .$$

Since α is directly proportional to f, each parameter scales with f as it scales with α.

We digress at this point to give some physical significance to this η-β-τ space. As can be seen from its definition above, β can be thought of as an "ejected mass-like" axis and τ can be thought of as an "age-like" axis. η can have a few different interpretations, but for our discussion it is best described as a "density-like" axis. The $\beta\tau$ plane is where the shape of the pertinent hydrodynamic variables, electron temperature and density as function of radius are determined. If we let λ be the ratio of the radius to the shock radius, then the temperature profile, $T(\lambda)$ and the density profile divided by η, $\eta^{-1}n(\lambda)$, are functions of β and τ only. Finally, α is measure of the mean x-ray surface brightness.

Various regions in the β-τ plane can be related to the different phases of the SNR evolution. An important quantity for discussing this demarcation is τ_s which is given by

$$\tau_s = .16\beta^{5/6} \quad .$$

When $\tau \sim \tau_s$ the remnant is in the so-called "free expansion phase". During this phase the ejecta dominates the hydrodynamics of the remnant which expands at a constant rate which depending upon the initial velocity of the ejecta. At $\tau = \tau_s$, the mass of the shocked ISM begins to exceed the mass of the ejecta, and the hydrodynamic profiles begin to approach those of the Sedov similarity solution for a point explosion (Sedov, 1959). The x-ray emission from the ejecta is significant for $\tau \lesssim 4\tau_s$. Beyond that time the contribution of the ejecta emission drops below a few percent of the total emission.

Increasing β increases the emission volume of the ejecta component relative to the emission volume of the shocked ISM and decreases the ratio of temperature

in the shocked ejecta to the temperature in the shocked ISM. For $\tau < \tau_s$ the temperature of the shock region is inversely proportional to β as well. Increasing τ for a fixed β means a larger fraction of the x-ray emission comes from the shocked ISM as shock wave sweeps up more interstellar matter. The temperature of the shocked ISM drops monotonically with increasing τ - slowly during the free expansion phase and like $\tau^{-6/5}$ during the Sedov phase. The temperature of the ejecta initially rises with τ during the formation of the reverse shock but later, at the times of interest for this work, it also decreases with increasing τ. For a fixed β and τ,η is a scaling factor for the density profile. $\eta\tau$ is proportional to $\int n_e dt$ which is the effective time for heating electrons in the "cold" electron model and the effective amount of time for evolving the ionization structure. Increasing η increases T_e/T_i (for Coulomb heating model only) and results in the ionization structure of the heavy elements to be closer to CIE.

Comparison with previous work

Early efforts for modeling non-equilibrium SNR, x-ray spectra were made by Itoh (1977, 1979). He constructed models with and without electron-ion thermal equilibration behind the shock front, but η and β were both fixed in his papers. The model in Itoh's 1979 paper was done with no ejecta at all. Concurrently with this model developed for this thesis. Shull (1982) and Hamilton, Sarazin, and Chevalier (HSC; 1982) have also devised similar models. Shull (1982) calculated models only with $\eta = 1$, with the no ejecta, and only with electron-ion thermal equilibration assumed. HSC calculate models varying in η and τ, for both electron-ion post shock equilibration and for only Coulomb electron heating, but again no ejecta contribution was considered. This work differs from these other efforts in that it includes the reverse-shocked ejecta as well as the shocked ISM.

The models by Itoh (1979), HSC, and Shull rely exclusively on a Sedov similarity solution to provide the hydrodynamic substrate. This latter approach is equivalent to this work when $\tau >> \tau_s$. In this "far Sedov" limit the spectrum is completely independent of β, and, as is done in Shull (1982) and HSC, τ can be converted to a shock temperature as follows:

$$T_s = 5.2\tau^{-6/5} \text{ keV} .$$

We also note that the definition of η is slightly different in HSC. For comparison

$$\eta_{jjn} = \left(\frac{\eta HSC}{10^{51} \text{ ergs cm}^{-6}} \right)^{1/3} .$$

This thesis also is among the first efforts at fitting spectral data with NIE models where η varys. (Shull and HSC currently have work in progress.)

These three other NIE models developed plus the one described here are nearly independent. At least two different methods for obtaining the hydrodynamic quantities, three or four different codes containing the atomic processes, and different codes for integrating the electron temperature and ionization structure were employed in these computer models. Despite these differences and many other idiosyncratic differences, all models seem to agree with each other where it is possible to check. For software systems of this size ($\sim 10^4$ lines of code) and subtle complexities (numerous) this is not a trivial statement.

The Far Sedov limit

The Sedov limit will be an important limit in this thesis and a convenient limit for discussing some of the properties of the process of mapping fitted parameters to physical parameters. In this limit,

$$T_{ev}' \approx 3.3 \times 10^{58} \eta^2 \tau^{6/5} \text{ cm}^{-3} ,$$

and

$$R_s' \approx 1.5 \times 10^{19}\ \tau^{2/5}\ \text{cm}$$

From these relations, α for a Sedov limit model is given as

$$\alpha = .1f\ \frac{\eta^2 \tau^{2/5} \theta^2_{\text{arcmin}}}{C_{13}}$$

where θ_{arcmin} is the angular radius in units minutes of arc and C_{13} is C_{ev} in units of 10^{13} cm^{-5}. f, again, is a filling factor. The distance is given by

$$D = 1\ B\ \frac{\alpha \tau^{2/5}}{\theta_{\text{arcmin}}}\ \text{kpc} \quad .$$

As can be seen from above, in the Sedov limit the final set of parameters scale quite differently with η, τ, and f:

$$E_o \sim \eta^5 \tau^{4/5} f^2 \quad t_3 \sim \eta^2 \tau^{7/5} f \quad D \sim \eta^2 \tau^{4/5} f \quad n_o \sim \eta^{-1} \tau^{-2/5} f^{-1}$$

The higher the powers to which η, τ, and f are raised the more severe the error propagation. So E_o is the least well determined while n_o is the best determined. This leads us to Nugent's Corollary of Murphy's Law of SNR modeling: "The more interesting a parameter, the more poorly it is constrained". While the blast energy, an important parameter for such issues as stellar evolution and nucleosynthesis of heavy elements, is typically uncertain by an order of magnitude, we can, with dazzling precision, measure the amount of garbage around the progenitor star.

In the way of a digression, the reader may be bothered that D is an output of the model as opposed to an input. In previous x-ray papers discussing SNR's,

the parameters known were T_e (from which T_s could be inferred under the assumption that $T_e = T_m$), the angular radius, and the x-ray flux. There were three equations relating these measured quantities to E_o, n_o, t, and D. Since there were four "unknowns", one had to be fixed so that the other three could be determined. Unless the age was known from historical records, the distance was usually the best determined "unknown". Heuristically speaking, with the advent of the NIE models another quantity, namely $\int n_e dt$, is measured from the amount of ionization heating and, possibly, from the amount of Coulomb heating. This gives a fourth equation so that all parameters can be determined.

Most distance estimates to SNR's rely on the empirical Σ - D technique using radio measurements. In some cases, additional estimates have come from analyzing historical records of the peak apparent magnitude of the supernovae event, or the progenitor star was a member of a certain star cluster. The use of NIE models in fitting x-ray spectral data represents an independent measure of the distance that arises from a non-empirical, physical model.

Caveats

Before proceeding to discuss the fits of the NIE model to x-ray spectral data, a few caveats are in order. First, despite the touting above, some care must be taken in accepting the inferred values of E_o, n_o, t, M_e, and D. Their rather fragile derivation could be destroyed by a number of systematic problems. Some of the problems that are suspected or are known to exist in SNR's include: inhomogenities may exist in the ISM; the ejecta/ISM interface is Rayleigh-Taylor unstable; and shocks might not form over the entire solid angle of the remnant. Heat conduction may be another important effect, especially if dense ejecta or ISM clouds are heated to shock temperatures. All of these may have a profound effect on the emergent spectrum. In addition to these hydrodynamic considerations,

systematic uncertainties in the atomic physics as well as detector modeling could also swamp any of the statistical uncertainties.

In order to put the NIE model in perspective, a brief review of the history of x-ray spectral modeling of SNR emission is helpful. At first, multi-temperature thermal bremsstrahlung models were fit to the data with the caveat that line emission and non-equilibrium effects were being ignored. Then as data and theoretical work improved multi-temperature CIE models that included the line emission were employed. The lack of line emission was no longer a problem but non-equilibrium conditions along with the number of problems outlined above still were. These models were taken to be parametrizations of the problem, but it was always the expectation of the observer that the parameters derived were indicative of the real remnant. With the introduction of the NIE model, the lack of consideration of the non-equilibrium effects has been removed. In light of the caveats given above, it is safest to still view the NIE model as a parametrization. To a rough approximation the model is representing a plasma with a characteristic electron temperature and an effective ionization time (possibly a second plasma if the ejecta is a significant component to the emission). As was discussed above, before NIE models the angular size, x-ray flux, and implied temperature were used to derive remnant parameters. The NIE model has added another measurement, the effective ionization time, and otherwise improved the derivation procedure; however, the basic idea is the same as before.

4.2 The Observation of MSH-14-63 (RCW86)

MSH 14-63 is the most likely candidate for the supernova recorded by the Chinese in A.D. 185 (Clark and Stephenson, 1977). While MSH 14-63 is the name of the radio source, an alias for the remnant is RCW 86, which is the designation of the optical filaments. Following the discovery of MSH 14-63 (Hill, 1967), other early radio maps clearly resolved a limb brightened shell with an angular radius of $\sim$20 arcmin (Caswell et al., 1975). Westerlund (1969a) suggested that the remnant was associated with an OB association. If this were the case, a Type II supernova would be indicated on the basis of stellar type. By using spectrophotometric studies, Westerlund determined the distance to the association to be 2.5 kpc. This measurement is in agreement with the measurement of the distance made by the Σ - D technique.

The first x-ray observation of MSH 14-63 was made by Naranan et al. (1977) in the range 0.5 to 2.5 keV using an experiment on the Apollo-Soyuz mission. The observation was taken in the range 0.5 to 2.5 keV. The spectrum in the range of 1 to 30 keV obtained from the OSO-7 spacecraft was reported by Winkler (1978). Winkler found that the combined spectrum of the two observations could not be explained by a simple thermal spectrum with a single temperature. Rather, two components each at different temperatures were needed to adequately explain the data. The temperature of the high-temperature component, which is presumed to be produced by the shocked ISM, was measured to be greater than 5 keV. The low temperature component, measured to be 0.22 keV, was attributed to the supernova ejecta which had been heated by inward propagating shock (McKee, 1974; Gull, 1973, 1975). Using this reverse-shock model, Winkler determined an ejected mass of greater than 5 $M_\odot$ is required. Winkler concluded that the x-ray spectral data supported the idea that MSH 14-63 was formed from a Type II supernova located in the OB association studied by Westerlund.

Because of increased spectral resolution and sensitivity of observations, most recent attempts to explain the SNR spectral data have employed more sophisticated models to predict the x-ray spectrum from hot, optically thin plasmas than the simple exponential spectrum used by Winkler. These models explicitly calculate the contributions from each element in the plasma to the continuum emission as well as the the line emission (Tucker and Koren; 1971, Kato, 1976; Raymond and Smith, 1977; Shull, 1981). For a large range of conditions of the plasma line emission from heave elements ($Z \geq 6$) dominates the spectrum, and as was discussed in the last chapter, a simplifying assumption that is often made is that the plasma is in collisional ionization equilibrium (CIE).

In this chapter we will present results of both CIE and NIE models with data collected from MSH 14-63 by the A-2 experiment on the HEAO-1 spacecraft.

Observations

The observations were made by two different detectors of the A-2 experiment (Rothschild et al., 1979) on board the HEAO-1 satellite. The low energy pulse height data (.5-3 keV) were obtained using the on-axis LED detector while the spacecraft was in a scanning mode. The high energy pulse height data (2-15 keV) were taken during a pointed observations using the MED detector.

Each detector had two separate co-aligned fields of view. Roughly, the dimensions of these two fields were 1°.5 x 3° full width at half maximum (FWHM) and 3° x 3° (FWHM). The data from both of these fields were combined to obtain the final data set used for the analysis. The dimensions of all the fields of view of the detector were larger than the dimensions of MSH 14-63 (diameter of 40 arcmin), so the data represent the integral over the entire surface brightness of the remnant.

The LED detectors had a sensitivity to photons as low in energy as 0.18 keV; however, because of contamination from α Centauri (Nugent and Garmire, 1978) the lowest energy data were not used. Since interstellar absorption of the spectrum from MSH 14-63 is so great at energies below 0.5 keV, this was not a significant loss of information. α Centauri is measured to have a steeply falling spectrum ($kT_e \lesssim 0.15$ keV) and in broad band measurements in the energy range above 0.5 keV α Centauri has a count rate $\lesssim .04$ that of MSH 14-63 (Nugent et al., 1982). These facts, combined with fact that the collimator transmission to α Centauri during the MSH 14-63 observations was $\lesssim 0.2$, gives us confidence that there has been no significant contamination of the pulse height data above 0.5 keV.

CIE Fits

We will first discuss fits of CIE models to the MSH 14-63 data-both a single temperature plasma and two-temperature plasma. There are three reasons for this digression:

1) Because bremsstrahlung and radiative recombination from hydrogen and helium dominate the spectrum at photons energies $\gtrsim 4.5$ keV, the electron temperature and reduced emission volume alone determine the shape and magnitude of the spectrum. The determination of the temperature, as we will discuss, will eliminate the Coulomb heating models.
2) Since only a two-termperature model was used by Winkler, we would like to apply the same model for purposes of comparison.
3) We would like to demonstrate how poorly a single temperature CIE model fits the data, before proceeding with NIE model fits.

Two-temperature CIE models assume two separate coronal plasmas of different temperatures. In addition to the temperatures and the reduced emission volumes of the two different components, other parameters are the elemental abundances

of the two components, and the interstellar absorption column, N_H.

The results of the fit are shown in Figure 1a. A reduced X^2 of 1.6 for 60 degrees of freedom is obtained. The only elemental abundance that was allowed to vary was iron. The results of the fit are shown in Table 1. The parameter of particular interest to this discussion is the higher temperature, ~.1 keV, which will be denoted, $T_{e,high}$. As mentioned above, at photon energies $\gtrsim$ 4.5 keV the spectrum is dominated by continuum emission from hydrogen - helium and, hence, $T_{e,high}$ is insensitive to NIE effects.

An important result from this value of $T_{e,high}$ is that we exclude the whole branch of NIE models which assume the electrons are heated by Coulomb collisions. Cox and Anderson (1982), using analytic approximations to the Sedov solutions for the temperature and densities in the interior of the remnant and analytic approximations for Coulomb heating, showed that the electron temperature is independent of radius for times shorter than $\sim 3000 E_{51}^{3/14} n_o^{-4/7}$. This "plateau" temperature as a function of time is given by

$$T_e \approx 1.5 \left(\frac{t}{1800 \text{ years}}\right)^{-2/25} \left(\frac{E_o}{10^{51} \text{ergs}}\right)^{4/25} \left(\frac{n_o}{1 \text{ cm}^{-3}}\right)^{6/25} \text{keV}.$$

In terms of our fitting parameters this equation becomes

$$T_e \approx 1.6 \, \tau^{-2/25} \, \eta^{2/5} \text{ keV}$$

As an example, Figure 2 shows the results of numerically modeling coulomb heating for $\eta = 0.2$ and $\tau = 1.2$. The two top graphs show the density and mean temperature shown with an analytic Sedov solution. The third graph shows the electron temperature assuming Coulomb heating only. The dotted line which displays Cox and Anderson's approximate solution demonstrates excellent agreement.

Because T_e is insensitive to the choice of parameters, an attempt to find a choice for D, E_o, and n_o that allows $T_e = T_{e,high}$ and satisfies the constraints for angular radius and reduced emission volume produces an absurd result. To wit: $D \sim 41$ Mpc, $E_o = 3 \times 10^{70}$ ergs, and $n_o = 6 \times 10^{-4}$ cm^{-3}. We will safely ignore the possibility, then, that the electrons are "cold" after having crosses the shock front.

Saying that there exists at the shock front some mechansim other than Coulomb interactions to couple the electrons to the ions does not prove that the mechanism will be sufficient to bring the electrons and ions into thermal equilibrium. If, after passing through the shock, the electrons have obtained a significant fraction but not the total amount of their equilibrium energy, then the time scale for them to reach equilibrium would still be as above. The only difference would be that the electron temperatures would be higher than those derived by Cox and Anderson (1982).

Before exploring the fits using the NIE models, we wish to emphasize that a single high temperature component does not fit the data at low photon energies. Figure 1b shows only the 5.1 keV component with a reduced emission volume as fitted in the two-temperature model. The flux at 1 keV differs from the predicted flux by a factor ~ 10.

Review of Parameters

Before discussing results of the model, we briefly review for the reader the definitions of the parameters used. The input parameters to the model and the units we will always use are the initial blast energy, E_o (units of 10^{51} ergs), the density of the interstellar medium around the progenitor star, n_o (units of 1 cm^{-3}), the amount of ejected mass from the progenitor star, M_e (units of $M_\odot$), the age of the remnant, t_3 (units of 1000 years), the abundance, relative to hydrogen, of elements in the ejecta (normalized to the measured solar value), the abundance,

relative to hydrogen, of elements in the ISM (normalized to the measured solar value), and the distance to the remnant, D (units of kpc). These parameters are mapped to more convenient set of parameters for purposes of the doing spectral fitting. There is a scaling parameter defined as

$$\alpha = \left(\frac{E_o}{n_o}\right)^{1/3}$$

and a number of "reduced" parameters:

$$\eta = (E_o n_o^2)^{1/3} = \alpha^{-2} E_o = \alpha n_o ,$$

$$\beta = \frac{M_e}{E_o} = \eta^{-1}\alpha^{-2} M_e ,$$

and

$$\tau = \left(\frac{n_o}{E_o}\right)^{1/3} t_3 = \alpha^{-1} t_3 .$$

A fourth reduced parameter is the reduced emission volume, C_{ev}, which is defined as

$$C_{ev} \equiv \frac{\int n_e^2 dV}{4\pi D^2} .$$

η, τ, β, and C_{ev} are derived from fits to the spectral data. α is then determined from the average x-ray surface brightness by

$$\alpha = \frac{\Sigma'(\eta,\beta,\tau)\theta^2}{C_{ev}} f$$

where Σ' is determined from η, β, and [illegible] action of solid angle of the remnant filled with shocked pla[illegible] of f will nominally be assumed to equal unity. With α, the input parameters are given by

$$E_o = \alpha^2\eta \quad M_e = \alpha^2\eta\beta \quad t_3 = \alpha\tau \quad n_o = \alpha^{-1}\eta$$

and the distance is given by

$$D = \frac{R_s'(\beta,\tau)\alpha}{0}$$

where R_s' is a constant determined from the fitted value of β and τ.

When $\tau \gtrsim 16\beta^{5/6}$ the remnant is in a Sedov phase and the shock temperature, T_s, can be given as a function of τ by

$$T_s = 5.2\ \tau^{-6/5}\ \text{keV} \quad .$$

Non-Ionization Equilibrium Models/$T_e = T_i$

We are going to assume for the balance of this paper that whatever mechanism is responsible for coupling electrons to ions at the shock front will bring them to equilibrium on an ignorably short time scale. Under this assumption then we will always assume that $T_e = T_i = T_m$.

The parameter β, as it turned out, is not a well constrained parameter for this data set. Results of fitting the data with models that have relatively high values of β will be discussed below; however, we will assume, for simplicity and definitiveness, during most of the discussion of the MSH 14-63 data that $\beta = 1$. Since the values of that fit the data under this assumption are $\sim$1.1, a deliberate consequence of this choice of β is that we will be working in the Sedov limit. There are three advantages to this:

1) Working in a regime of parameter space where emission from the shocked ISM dominates the spectrum is deemed preferable to working in regime where the reversed shocked ejecta was dominant since the modeling of the latter is more controversial.

2) Since the spectrum is insensitive to β in this limit, the results of the fit are also insensitive to the precise choice of β, other than it is sufficiently low.

3) Models that are in the Sedov limit make possible direct comparisons with the work of Shull (1982) and Hamilton et al. (1982).

In addition to fitting for C_{ev}, N_H, η, and τ, we also allowed the abundances for Fe, S, and Si to vary. The abundances for the rest of the elements were fixed at solar values as given by Allen (1976). The results of the best fit are displayed in Table 2 along with the input parameters inferred from assuming the radius of the remnant to be 20 arcmin. Figure 3 shows a display of the best fit and an insert showing the dependence of X^2 on η and τ. This X^2 grid is calculated by fixing the values of η and τ and letting the balance of the parameters vary. The inner contour is for change of X^2 from minimum of 4.6 which corresponds to the minimum volume 90% confidence region for 2 parameters (Lampton et al., 1976). For comparison, a contour for $\Delta X^2 = 10$ is also shown. The results of fits that are done at two extremes of the 90% region are shown in Table 2.

We will now discuss various aspects of this fit:

Elemental Abundances

The over-abundance of the S and Fe was needed primarily to fit the K_α lines at 2.4 and 6.7 keV. Because L shell emission from iron is a major contributor to the spectrum at $\sim$1 keV, the reader may be concerned that the overabundance was required to match the flux in the LED data. To demonstrate that this is not the case and that a solar abundance composition can fit the data with the exception of the lines, we have also performed a fit where all the elemental abundances in the NIE model were fixed at solar, and lines were inserted, ad hoc, at the K_α energies of S, Fe, and Ar (2.4, 3.0, and 6.7 keV, respectively) to compensate for the missinf flux at those photon energies and in effect neutralize the influence of the lines in the fit. The results of the fit are given in Table 3 and the fit shown in Figure 4.

The effect of changing the Fe abundance does have an effect on other parameters. In this case, increasing η has the effect of compensating for the lowered elemental abundances since the population of Fe XVII and Fe XVIII, both important 1 keV L-shell emitters, increase dramatically as η is raised from 0.15 to 0.3.

Density, age, and N_H

The fit to the combined LED/MED data gives good agreement to other known properties of MSH 14-63. The density of 0.1-0.3 is reasonable for the height of the remnant off the galactic plane ($\gtrsim$ 80 (D/2kpc)pc). The measured value of N_H would imply an average hydrogen density along the line of sight to the remnant of $\sim$0.7 (2 kpc/D). This is also a reasonable value considering the angle of the remnant off the galactic plane.

Most importantly, the fitted values of the age are in reasonable agreement with the age of 1800 years known from Chinese astronomical records. Alternatively, if one assumes an age of 1800 years, then the average x-ray surface brightness is consistent the measured value. This not a trivial statement since the average x-ray surface brightness scales as η^2. A large fraction of the volume of the remnant cannot be filled with a plasma which had a much higher η than those fitted above.

Fe K_α line

The Fe K_α is an attractive feature for study because it is prominent and measurement of the surrounding continuum is easy. The line is composed of a blend of lines around $\sim$ 6.6 keV from many different ionic species of iron. There are two anomalies concerning the line in the NIE model:

1) An over-abundance of iron must be assumed to explain the equivalent width of the feature.
2) The centroid of the line feature in the data is apparently shifted to higher energies with respect to the predicted line feature. These shifts in the centroid are $\sim$ 150 eV to lower energies. Doppler shifts can probably be ruled

out since the shock velocity implied from the x-ray temperature could at most produce a shift of ∿40 eV if all the iron-line emitting material wa on the far side of the remnant.

In a 5 keV plasma which is in CIE, the most prominent lines arise from H-like and, more so, He-like ions, but when the plasma is out of CIE the populatio. of these ions can be severly diminished. Given the ionization time, ($\int n_e dt$) in MSH 14-63, predicted by the above NIE fits the prominent iso-sequences are S-like to F-like ions. The emission, which results following innershell ionizations of these ions, has photon energies of ∿200 eV lower then the characteristic Kα radiation from He-like and H-like ions. At greater ionization times the ionization structure becomes more advanced. The characteristic energy of the line photons increases with increasing ionic charge. The efficiency of ions below C-like for producing K_α is generally lower than the strong He-like ion by a factor of ∿3. The C, B, and Be-like ions, on the other hand, produce comparable amounts of Kα from innershell excitations via dielectronic recombination.

To reconcile the observed iron feature in the MSH 14-63 data two requirements in some region are required. First, in order to produce Fe Kα emission at all, $T_e \gtrsim 5$ keV. Second, the effective ionization time would have to be $\gtrsim 5$ times that of the models used in the fits above. The latter requirement is necessary to start populating the ionic states at or above the C-like isosequence. The characteristic radiation from these ions is not only at higher photon energies, but again, these ions also have higher efficiencies for producing Kα.

In order to quantify this discussion, we will perform NIE model fits on just the data $\gtrsim$ 4.5 keV. Using these data will avoid many assumptions involved with fitting the data at lower energies which are dominated by line emission. We will consider only four parameters: n, τ, C_{ev}, and the abundance of iron, A_{Fe}. The amount of N_H, which only marginally affects the data at these energies was fixed

at the fitted value from above and the abundances of all other elements were fixed at solar. In way of review before proceeding, τ is primarily responsible for the shape of the continuum, $\eta\tau$ is proportional to $\int n_e dt$, A_{Fe} is proportional to the equivalent width (strength) of the line, and C_{ev} acts as an overall scale factor. τ and C_{ev} are well determined by the continuum and will not change by more than 10% for this discussion.

Figure 5a shows a fit done with η fixed at 0.2 and the balance of the parameters left to vary. The non-iron contributions to the spectra have been subtracted. As noted above, the model shows a distinct shift of $\sim$ 150 eV to lower energies and an abundance enhancement of factor of 3.2 over solar is needed to explain the intensity of the feature. If we now unpin the value of η, a best fit is obtained with a value of $\eta = 3.1$. This fit is displayed in Figure 5b. Not only does the line fit better at this value of η (The improvement in X^2 was $\sim$ 11), but it does so with an abundance much closer to solar. The 95% confidence region (2σ) for η ranged from 1 to 6. (Even at $\eta = 6$ there are still significant deviations for CIE.)

Finally the same region was fit with a CIE model. Now a single electron temperature, T, has replaced τ. The fit displayed in Figure 5c, also shows a well centered line with near solar abundance; however, the CIE model predicts too much emission at $\sim$ 8 keV. This line feature, which has been referred to as Kβ (e.g. Pravdo and Smith, 1979), contains n=3 to n=1 transitions from H-like and He-like Fe and Kα emission from Ni. The Fe component tends to dominate because Ni is less abundant than Fe by a factor of $\sim$18. The ratio of Kβ to Kα has been used by Pravdo and Smith as a diagnostic for CIE since it is very sensitive to the population of the He and H-like ions in Fe. The X^2 of the fit to data points between $\sim$ 5.5 keV and $\sim$ 9 keV increased by 12.1 from best fit NIE to best fit CIE. This increase, which is evidence against the plasma being in CIE, came primarily from contributions around the Kβ feature.

Taking the best fit value of η from the Fe-line fits what can one say about the remnant? First, because the surface brightness (or α) scales as η^2, we can rule out a model where plasma of this nature fills the entire volume of the remnant. For filling factors near unity, the distance would need to be 200 kpc and the age, 3×10^6 years. Filling factors of $\sim$1% would be adequate, although we know from x-ray images probably 50-75% of the remnant is filled with plasma. These x-ray images (Pisarski, private communication) show a limb brightened shell that has large variations in surface brightness as a function of angle around the ring - the brightest region behind in the SW. In addition there are noticeable deviations from a circular ring. There is some correlation for brighter regions to have a smaller radius of curvature. All of this suggests that there probably are density inhomogenities on various different size scales present in the remnant.

Since the models calculated above assume a homogeneous ISM, they are what we would call "single-η" model. What the spectral data and the x-ray image seem to require is, in a sense, a "multi-η" model. Somewhat analogous to "two-temperature" models, we would argue for low η's to explain the shape and flux of the low energy emission and high η's to explain the shape and flux of the high energy lines.

The high-η components could for example be explained as dense cloudlets that are heated by conduction to temperatures of the post-shock region. Another possible source of material in the remnant with high ionization time is the ejecta. The reverse shock cannot be the source of the Kα emission since the temperatures are not high enough (McKee, 1974; Gull, 1974, 1975). There have been two mechanisms suggested for mixing the ejecta into the hotter, shocked ISM regions - neither was appropriate for inclusion in one-dimensional hydrodynamic model. If the ejecta was initially in a smooth shell, the contact surface between the shell and the shocked ISM would become Rayleigh-Taylor unstable (e.g. Gull 1975). Fingers of this dense ejecta material could then break away

from the rest of the ejected material and be heated to temperatures comparable to the shocked ISM by heat conduction (Chevalier, 1975). Alternatively, some of the ejecta could initially be in clumps to begin with (Chevalier 1977). In addition to being heated by shock waves due to pressure differences between the clump interior and the shocked ISM, the higher temperatures could, again, be obtained by heat conduction.

Distance

We turn our attention next to the question of the distance to MSH 14-63. As mentioned in the introduction, Westerlund (1969a) has measured the distance to an OB star association in the direction of MSH 14-63 by spectrophotometric technique. He finds a distance modulus of 12.0 ± 0.2 which corresponds to a distance 2.5 kpc with an uncertainty of roughly 0.2 kpc. This is inconsistent with the distances related to the x-ray measurements discussed here which argue for the distance being much closer ($\sim$1.6 kpc).

Given that the age is known, the best method for discussing the limits on the distance by x-ray measurements is, again, to work only with data above 4.5 keV. Here the only assumptions are that the remnant can be approximated by a Sedov blast wave, that the electron temperature is equal to the mean temperature, that the age is 1800 years, and that the angular radius of the shock front is 20 arcmin. The distance is then given as

$$D = 1.6 \left(\frac{\theta}{20 \text{ arcmin}}\right)^{-1} \left(\frac{t_3}{1800 \text{ years}}\right) \tau^{-3/5} \text{ kpc.}$$

The minimum volume 95% conficence region (2σ) in τ extends from 0.9 to 1.2. The lower limit of 0.9 (an upper limit on the shock temperature of $\sim$6 keV) gives an upper limit on the distance of 1.7 kpc. For the x-ray determined distance to agree with Westerlund result would require $\tau \gtrsim 0.55$ (plasma temperatures of 12-15 keV), which can be ruled out. It is, of course, possible that the progenitor

for MSH 14-63 was not a member of Westerlund's OB association; however, we do point out that any deviations from the assumptions stated above would tend to make us underestimate the distance.

First, even though the longest angular dimension of the x-ray emission is 40 arcmin, the brightest regions - those dominating the x-ray spectra - appear to have a smaller radius of curvature, maybe as small as 15 arcmin. Second, if, despite some non-Boulomb electron heating at the shock front, T_e is still less than T_i, than the shock temperature would be underestimated by our measurement of T_x. Finally, the introduction of density inhomogenities into the remnant can alter the interpretation. If, for example, after expanding for a significant part of its lifetime, the shock in the SW part of MSH 14-63 moved into a denser region, the shock temperature would be lower than the radius would imply. Finally, while a temperature of 12-15 keV can be ruled out if the x-rays were all arising from a post-Sedov shock, a thin, hot component related to the postshock regions could exist that was being overwhelmed by cooler emission from denser regions. The observations lack the sensitivity to detect such a hot component under these conditions.

A lower limit can be set for the distance by assuming that the remnant is still in the early free expansion phase. A lower limit of the kinetic temperature of the shock of 5 keV would imply a constant expansion velocity of 2100 km s^{-1}. Assuming, again, an age of 1800 years and an angular radius of 20 arcmin yields a lower limit on the distance of 700 pc.

Emission from the ejecta

The value of β has consequences for demonstrating the existence of the reverse-shock ejecta component and measuring the mass of the ejected material. As was mentioned above, β was not a well constrained parameter. We fit the data with values of β ranging from 1 to 10 with no more than a change of roughly unity in the value of X^2. At low values of β the ejecta was only a few percent of the

total emission at $\sim$ 1 keV and, thus, did not significantly effect the spectrum. At higher values of β the fraction of emission from the ejecta became dominant but the temperature of the ejecta decreases. The ejecta's dominance of the spectrum occurred at less than 0.5 keV where interstellar absorption makes observations difficult. The amount of emission from the ejecta was comparable to the shocked ISM at $\sim$ 1 keV, but as with discussion on the iron abundance, varying the value of η, which varied the contribution to the $\sim$ 1 keV emission from the shocked ISM, could compensate for any changes in the ejecta emission. In low resolution we were not able to decouple the components.

Using much the same argument for providing a lower limit to the distance we can put an upper limit on the size of β of $\sim$ 40. Any value higher than that would produce shock velocities that were too low to produce a 5 keV plasma during the lifetime of the remnant.

Blast Energy

Knowledge of the blast energy has a direct application to accessing whether the progenitor of MSH 14-63 is a Type I or Type II supernova. The issue of the association of MSH 14-63 with the OB star group also relate. the question of the type of SN explosion that formed the remnant. The association would strongly suggest that the MSH 14-63 was a Type II supernovae (Shklovsky, 1962), since Type II supernova are thought to occur in massive stars.

The results of the standard NIE model with β fixed at unity which are given in Table 2 would indicate that the blast energy, E_o, was $\lesssim 6 \times 10^{50}$ ergs. However, as the discussion in Chapter 2 pointed out, E_o is a very sensitive function of η. Fixing the abundances to solar, for example, moved the inferred value of the blast energy up to $\sim 1.2 \times 10^{51}$ ergs. This large range of uncertainty in E_o along with the large range of uncertainty in the mass of the ejecta, M_e does not allow an unambiguous assertion as to the type of supernova explosion.

[Fe XIV] Emission

Lucke et al. (1979) have made measurements of the [Fe XIV]λ5303 emission line in RCW86. They observed a flux of $2.28 \pm .98 \times 10^{-14}$ ergs cm^{-2} s^{-1} from summing four 5 arcmin circular fields in the SW part of the remnant at the shock front. The dereddened flux was given as 1.4×10^{-12} ergs cm^{-2} s^{-1}. In CIE, [Fe XIV] emission peaks rather sharply at 2.1×10^6 K. For CIE plasmas with $T_e \lesssim 1.5 \times 10^6$ K or $T_e \gtrsim 3.0 \times 10^6$ K the emissivity of the λ5303 line drops precipitously as a function of temperature. The authors interpreted their observation in terms of the two-temperature model fit to the x-ray data. They ignored the high-temperature blast-wave component, because under the assumption of CIE the amount of [Fe XIV] emission would be negligible at the measured temperature of 6×10^7 K. Rather, they suggested associating their flux with the alleged low-temperature x-ray component ($2.5 < T_6 < 6$) or an even lower temperature component which they argue would be difficult for x-ray detectors to detect because the bulk of this emission would be attenuated by photoelectric absorption in the intervening ISM.

Though it is possible that these low temperature components exist, we would like to put forth an argument that ignoring the high-temperature blast wave is not justified. Because of the time-dependent nature of the ionization behind the shock, a shell of [Fe XIV] is produced which has sufficient emission volume as to produce a flux comparable to that observed.

The unattenuated [Fe XIV] λ5303 flux observed at the earth, S, from the blast wave of a remnant at a given time is

$$S = \frac{4\pi \int_0^{R_s} n_e^{\,2} P_{14}(T_e) A_{Fe}\, X_{14} \tau^2 dr}{4\pi D^2}\, f_{ob}$$

where R_s is the shock radius, n_e is the electron density, P_{14} is the emissivity of the line assuming a solar abundance for the iron (from Allen, 1976) and 100% concentration of the iron in the [Fe XIV] ionic state, A_{Fe} is the abundance of iron in units of solar, X_{14} is the fractional concentration of the [Fe XIV] ionic state, r is an integration variable, D is the distance to the remnant, and f_{ob} is a correction for a beam size less than the size of the remnant. X_{14} and n_e^2 are the most rapidly changing quantities behind the shock so we approximate the equation for S as

$$S = C_{ev}\, f_{ob}\, A_{Fe}\, P_{14}(T_e)\langle X_{14}\rangle$$

where $\langle X_{14}\rangle$ is the emission weighted average of the X_{14} and is given as

$$\langle X_{14}\rangle = \frac{\int_0^{R_s} n_e^2 X_{14} r^2 dr}{\int_0^{R_s} n_e^2 r^2 dr}$$

The [Fe XIV] λ5303 line results from the forbidden transition $3s^2 3P\ ^2P_{1/2} - {}^2P_{3/2}$. Population of the $^2P_{3/2}$ level results from direct electron excitation of the ground state or from cascades following electron excitation to higher energy levels. In general, the emissivity, for an atomic line from an element with nuclear charge Z and ionic charge z, in an optically thin plasma of temperature T_e, and resulting from electron collisional excitation is given by

$$\frac{P}{n_e^2} = X_{Z,z} \left(\frac{n_Z}{n_H}\right) 1.71 \times 10^{-19}\, T_6^{-1/2}\, \Sigma_{eff} \left(\frac{E}{I_H}\right) e^{-\frac{E_{xz}}{kT_e}} \text{ ergs cm}^{-2}\ \text{s}^{-1}$$

where $X_{Z,z}$ is fractional ionic concentration, (n_Z/n_H) is the number fraction of the element relative to hydrogen, (E/I_H) is the energy of the emitted photon in rydbergs, Σ_{eff} is the effective collision strength, E_{ex} is the excitation energy,

and T_6 is the electron temperature in units of 10^6 K. To arrive at P_{14}, the fractional ionic concentration is set to unity, the exponential factor is set to unity because $kT_e >> E_{ex}$, and the elemental abundance is taken from Allen (1973). A value for Σ_{eff} of $\sim$3 is obtained by extrapolating from a graph given in Nussbaumer and Osterbrock (1970). Σ_{eff} includes cascades following excitation to higher levels. The resulting expression for P_{14} is

$$P_{14} = 3.51 \times 10^{-24} \left(\frac{T_e}{10^6 K}\right)^{-1/2} \frac{\Sigma_{eff}}{3} \text{ ergs s}^{-1} \text{ cm}^3 .$$

We will also include λ5303 photons produced following ionizations of Fe XIII to FE XIV. Using branching ratios given by Nussbaumer and Osterbrook (1970), we calculate that 46% of the ionizations will result in λ5303. Taking ionization rates from Raymond and Smith (1977), we can calculate an analogous expression to P_{14} for P_{13}:

$$P_{13}(T_e \gtrsim 10^7 K) = 3.4 \times 10^{-26} \text{ ergs s}^{-1} \text{ cm}^3 .$$

We use a nominal value of 5×10^7 for T_e and 1.4×10^{13} cm^{-5} for C_{ev}. For the calculation of $\langle X_{14} \rangle$ we will assume that at the shock, at least, a low η model as valid. For $\eta = 0.16$ and $\tau = 1.2$, $\langle X_{14} \rangle \simeq 0.18$ and $\langle X_{13} \rangle \simeq 0.16$. We estimate f_{ob}, which is fraction of emission volume observed, to be 0.07. This calculation of f_{ob} incorporated effects of limb brightening. These values given S equal to $9 \times 10^{-14} A_{Fe}$ ergs cm^{-3} s^{-1}.

This number is less than the measured value by a factor of $\sim$13, but three good possibiiities that could bring the calculation more into agreement are:

1) The iron abundance of the shocked material could be high by a factor of 2-3 times solar.

2) Lucke et al. observed in the region of the most intense x-ray emission. This implies that the post-shock densities might be higher in this region. Higher densities shrink the X_{14} by a factor of n_e^{-1}, but they increase the surface brightness, which is proportional to $C_{ev}f_{ob}$, by n_e^2. The resulting value of S scales like n_e.

3) The Lucke et al. measured value for S is dependent on dereddening. They took 2 mag of extinction from the measurements by Westerlund (1967) which assume that the remnant is in the OB Association. If it is closer as the x-ray data suggest, the reddening correction would be lower than the one used.

Given the uncertainties in the input parameters, statistical uncertainties, and uncertainties in the dereddening, this predicted flux might be consistent with the one measured. At the very least, the [Fe XIV] flux from the high temperature blast wave component cannot be dismissed as lightly as Lucke et al. suggest if the plasma is not in CIE. For comparison, we note that the value of S assuming CIE in a $\sim$ 5 keV plasma is decreased $\sim$ 20 orders of magnitude from the NIE result.

Conclusion

In summary, the results of this chapter are the following:

1. A significant non-Coulomb, ion-electron interaction is occurring in the remnant, presumably at the shock front.
2. The data can be fit by a model with little or no emission from any source other than the shocked ISM with an age which is consistent with that of MSH 14-63.
3. Anomalous abundances of heavy elements and possible discrepancies in the centroid and shape of the Fe K_α feature could be explained by inhomogenities in the ISM density or by ejecta that have come to thermal equilibrium with the shocked ISM.
4. Under the assumptions of the model, the distance to the MSH 14-63 is inconsistent with distance measured to an OB association in the direction of the

remnant; however, plausible deviations in the model assumptions might explain the discrepancy.

Future observations with good combined spectral and spatial resolution, especially at Fe K_α would be helpful in addressing the issues raised here.

Table 1	
Two Temperature Model	
$C_{ev,low}$	$8.1 \pm 1.6 \times 10^{12}$ cm^{-3}
$T_{e,low}$	0.52 ± 0.04 keV
$C_{ev,high}$	$7.1 \pm 0.2 \times 10^{12}$ cm^{-3}
$T_{e,high}$	5.1 ± 0.14 keV
N_H	$1.1 \pm 0.3 \times 10^{21}$ cm^{-2}

Table 2

NIE Model ($T_e = T_i$)

	best fit	~ limits	
C_{sv} (10^{13} cm^{-5})	1.4	1.6	1.2
η (foe$^{1/3}$ cm^{-2})	0.16	0.12	0.22
β ($M_\odot$ foe^{-1})	1 (fixed)	-	-
τ (kiloyears cm^{-1} foe$^{-1/3}$)	1.2	1.3	1.1
N_H (10^{21} cm^{-2})	4.4	4.7	4.1
A_{Si} (solar)	0.7	0.6	0.8
A_S (solar)	3.4	4.1	2.8
A_{Fe} (solar)	3.9	4.8	2.6
χ^2_ν ($\nu = 53$)	1.3	1.4	1.4
α (foe$^{1/3}$ cm)	0.76	0.33	1.7
E_0 (foe)	0.09	0.01	0.6
n_0 (cm^{-3})	0.2	0.4	0.1
t_3 (10^3 years)	0.9	0.4	1.9
D (kpc)	0.7	0.4	1.6

cb. foe $\equiv 10^{51}$ ergs (fifty-one ergs; ☺ Hans Bethe)

Table 3

NIE Model with K^{α} lines

	best fit
C_{sv} (10^{19} cm^{-5})	1.2
η (foe$^{1/3}$ cm^{-2})	0.30
β ($M_\odot$ foe^{-1})	1 (fixed)
τ (kiloyears cm^{-1} foe$^{-1/3}$)	1.1
N_H (10^{21} cm^{-2})	3.5
χ^2_ν (ν = 53)	1.3
a (foe$^{1/3}$ cm)	2.8
E_0 (foe)	2.4
n_0 (cm^{-3})	0.11
t_3 (10^3 years)	3.1
D (kpc)	2.9

Figure Captions

Figure 1

(a) shows a fit to the data using a two-termperature CIE model. Histogram represents best fit model and the crosses are the data points. (b) shows only the high temperature CIE model.

Figure 2

An illustrative example of electron temperature profile when only Coulomb heating is considered is given in (c) from calculations by NIE model. Cox and Anderson (1980) approximate analytic solution is denoted by the broken line. The density and mean temperature profiles are shown for comparison in (a) and (b), respectively. Histograms are calculations from the NIE model and the smooth curves is calculated from the analytic solution for a adiabatic remnant.

Figure 3

The best fit model (histogram) using NIE model is shown with the data points. Insert is the projection of X^2 space on the $\eta - \tau$ plane. Contours show the change of X^2 from the best fit. Both 4.6 and 10 are shown.

Figure 4

Same as Figure 3 but now lines have been inserted at the Kα energies of S, Ar, and Fe (2.4, 3.0 and, 6.7 keV, respectively). The abundances of the elements in the NIE model were set to solar.

Figure 5

These graphs represent fits to the data at photon energies $\gtrsim$4.5 keV where the non-iron contributions to the model have been subtracted to emphasize the fit of the model at the Fe Kα feature. (a) shows the best fit when η is fixed at 0.2, (b) is the best fit letting all parameters vary, and (c) is a fit with a CIE model. Fitted abundances, A_{Fe} are given in the figure.

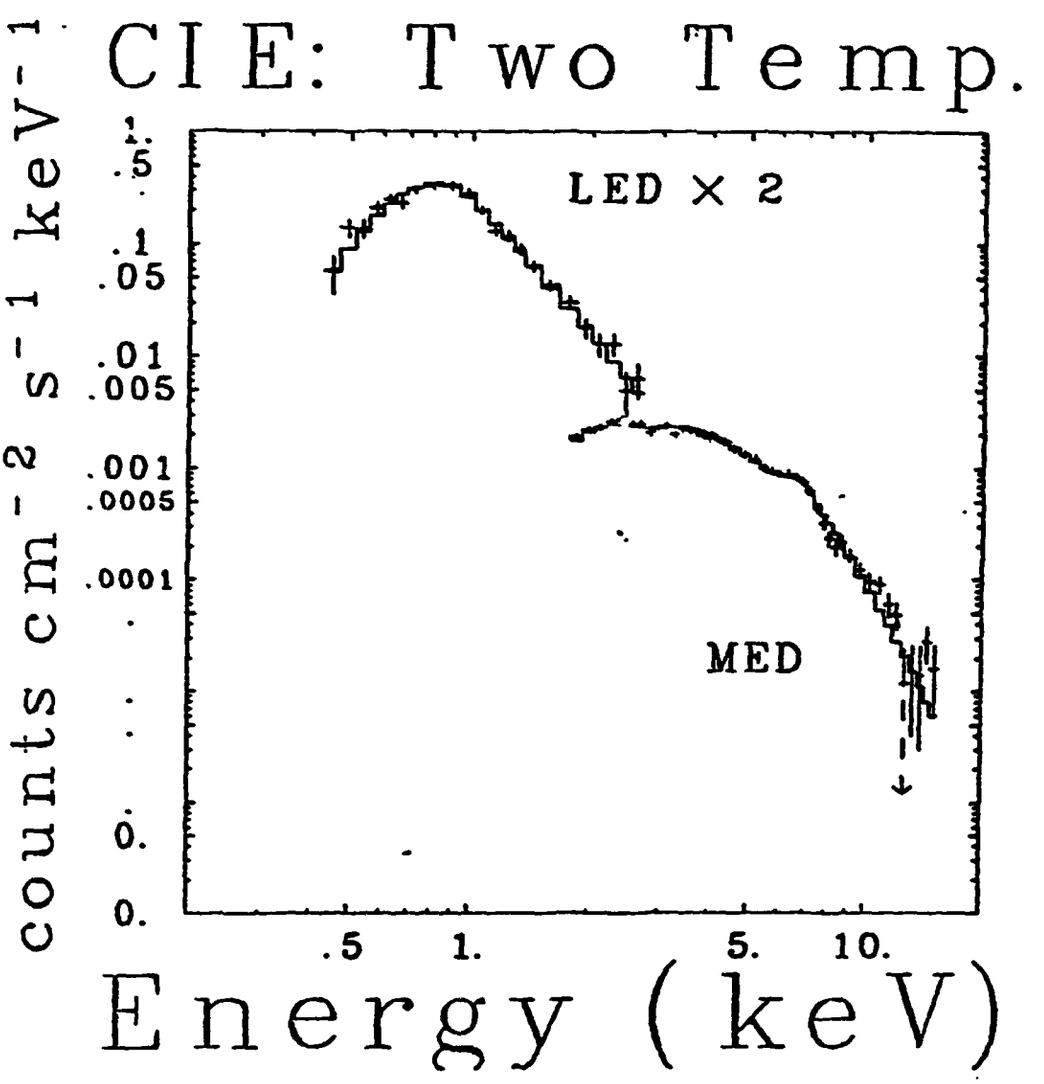

Figure 1a

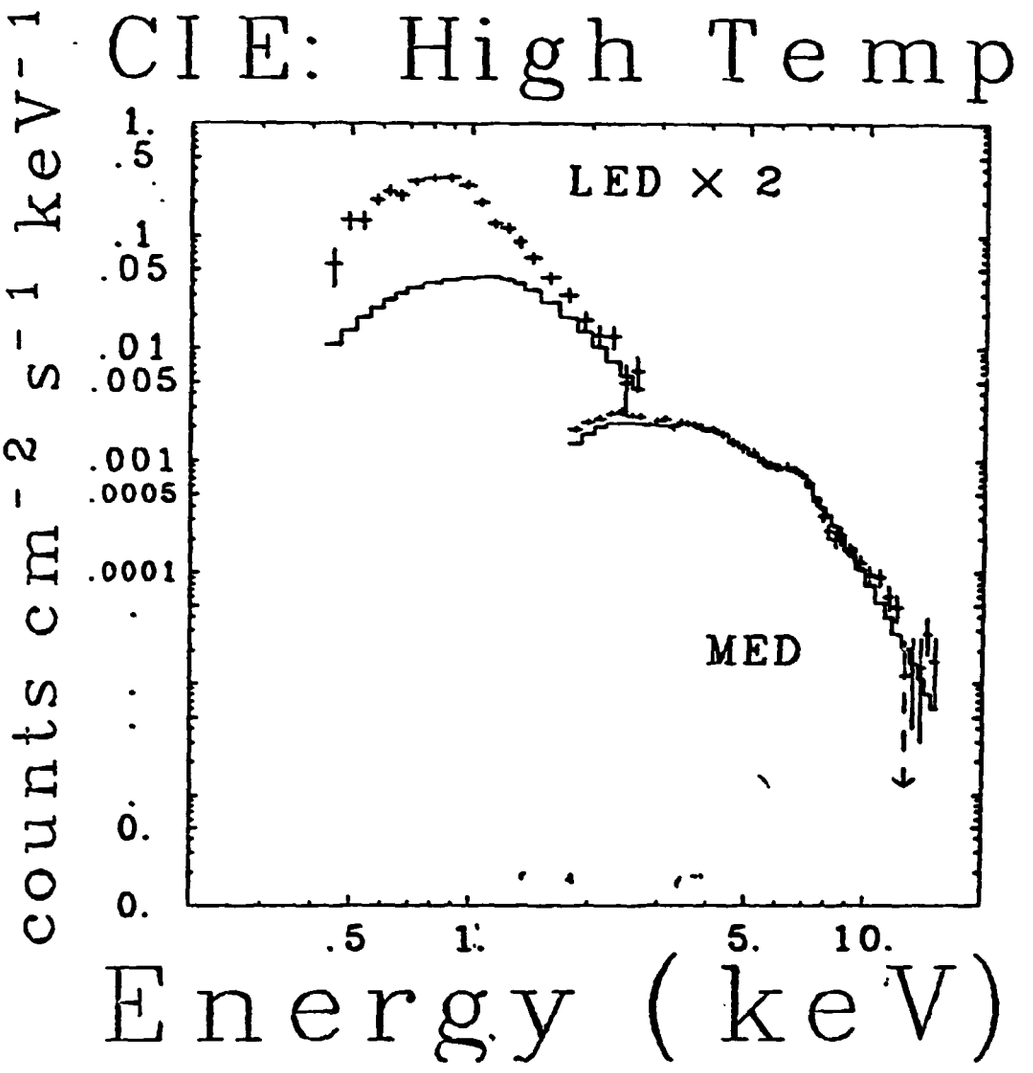

Figure 1b

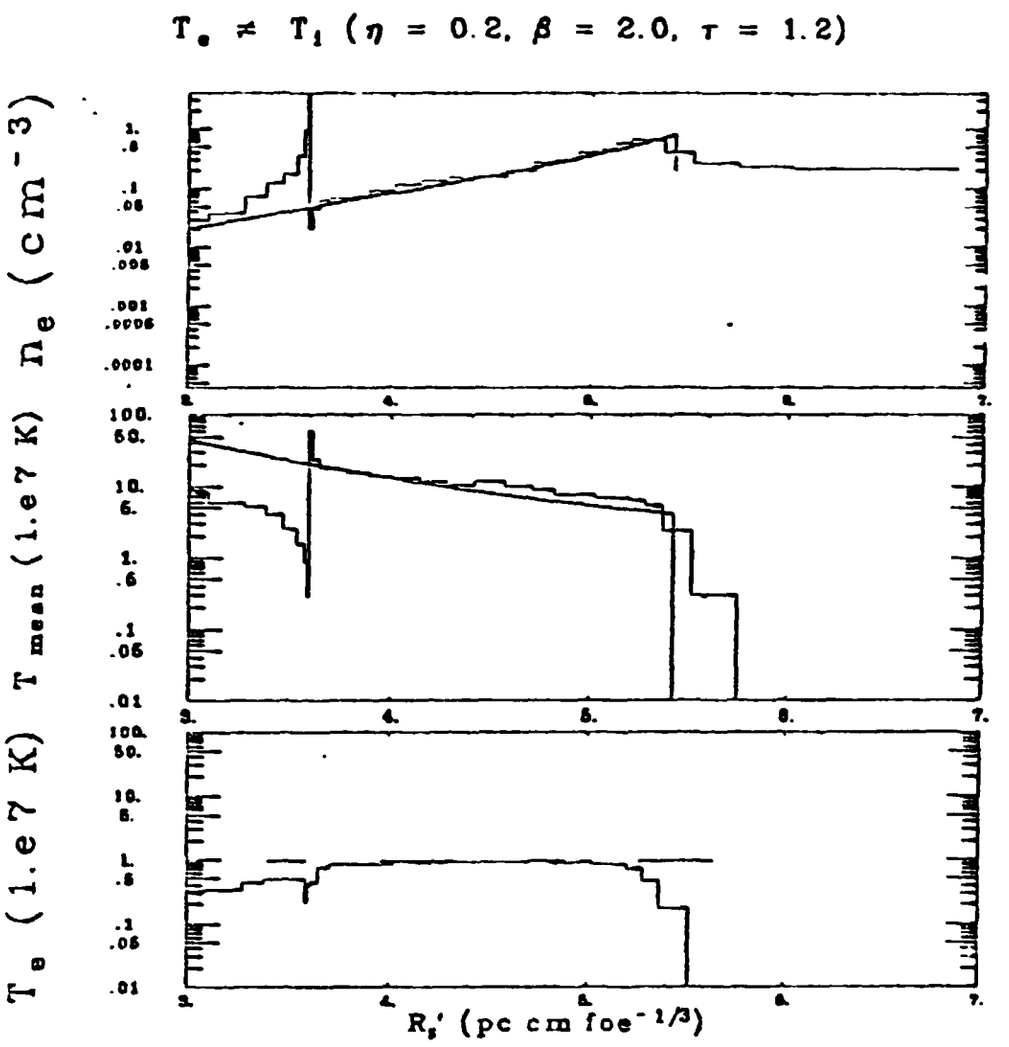

Figure 2

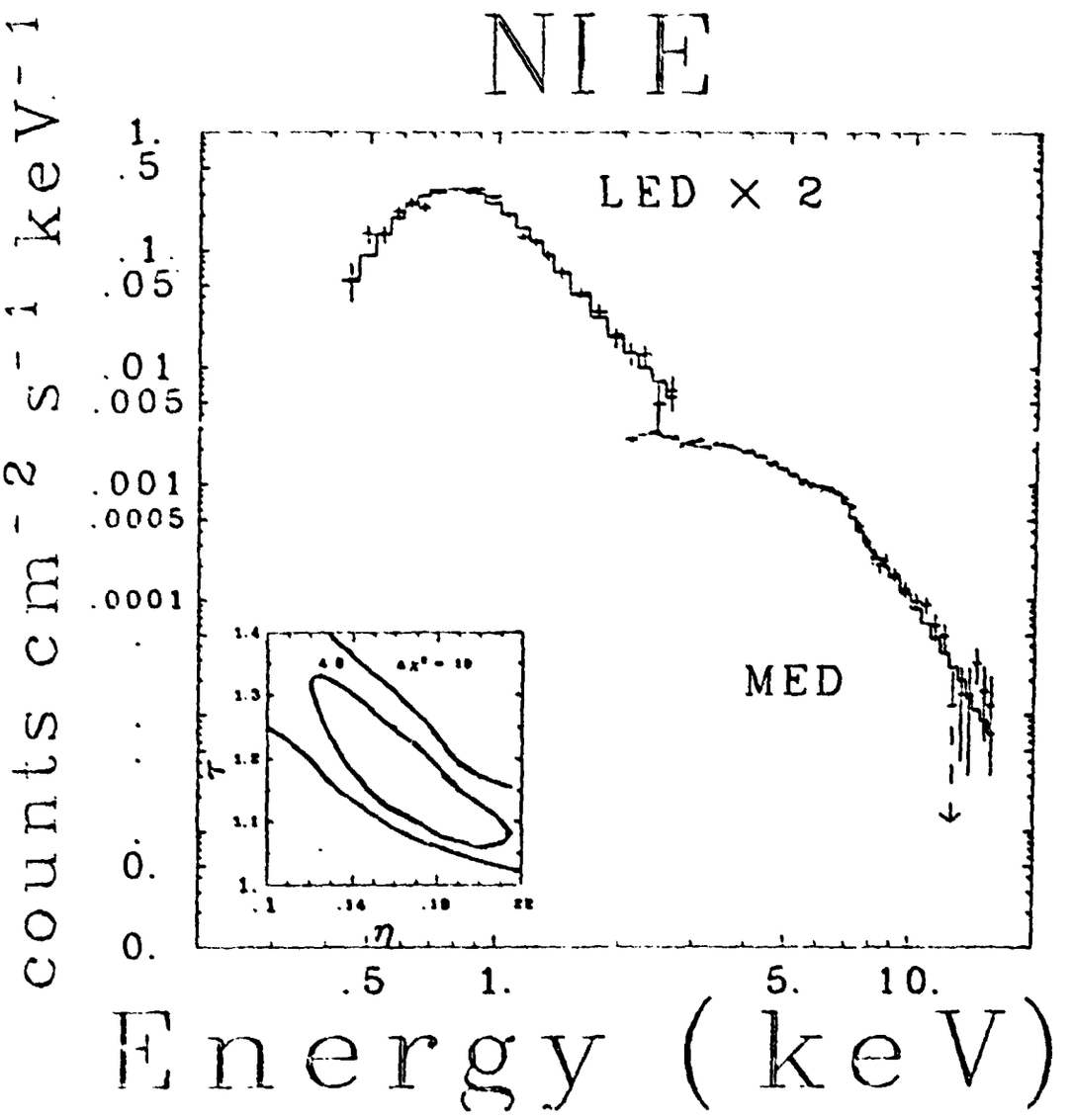

Figure 3

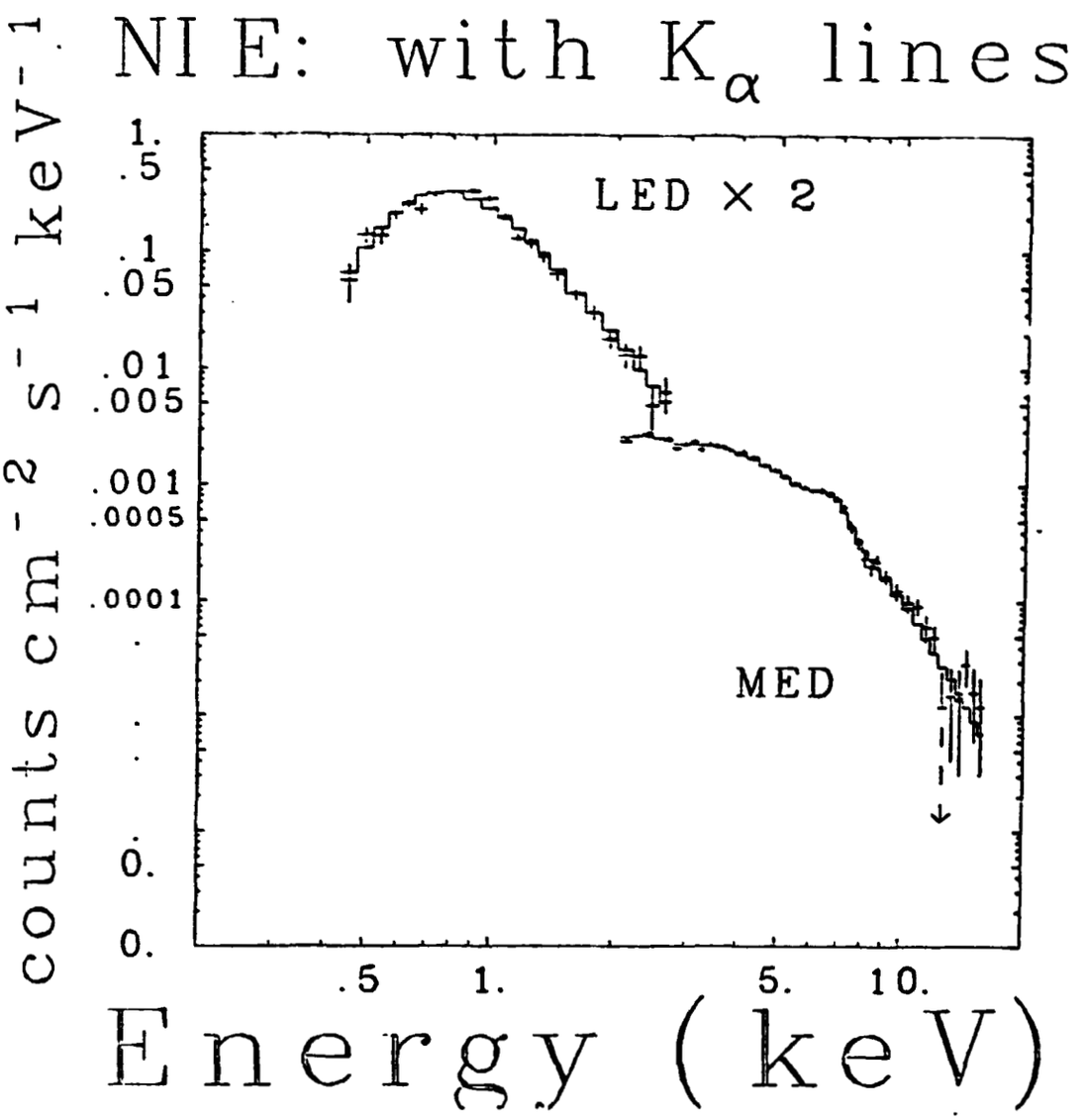

Figure 4

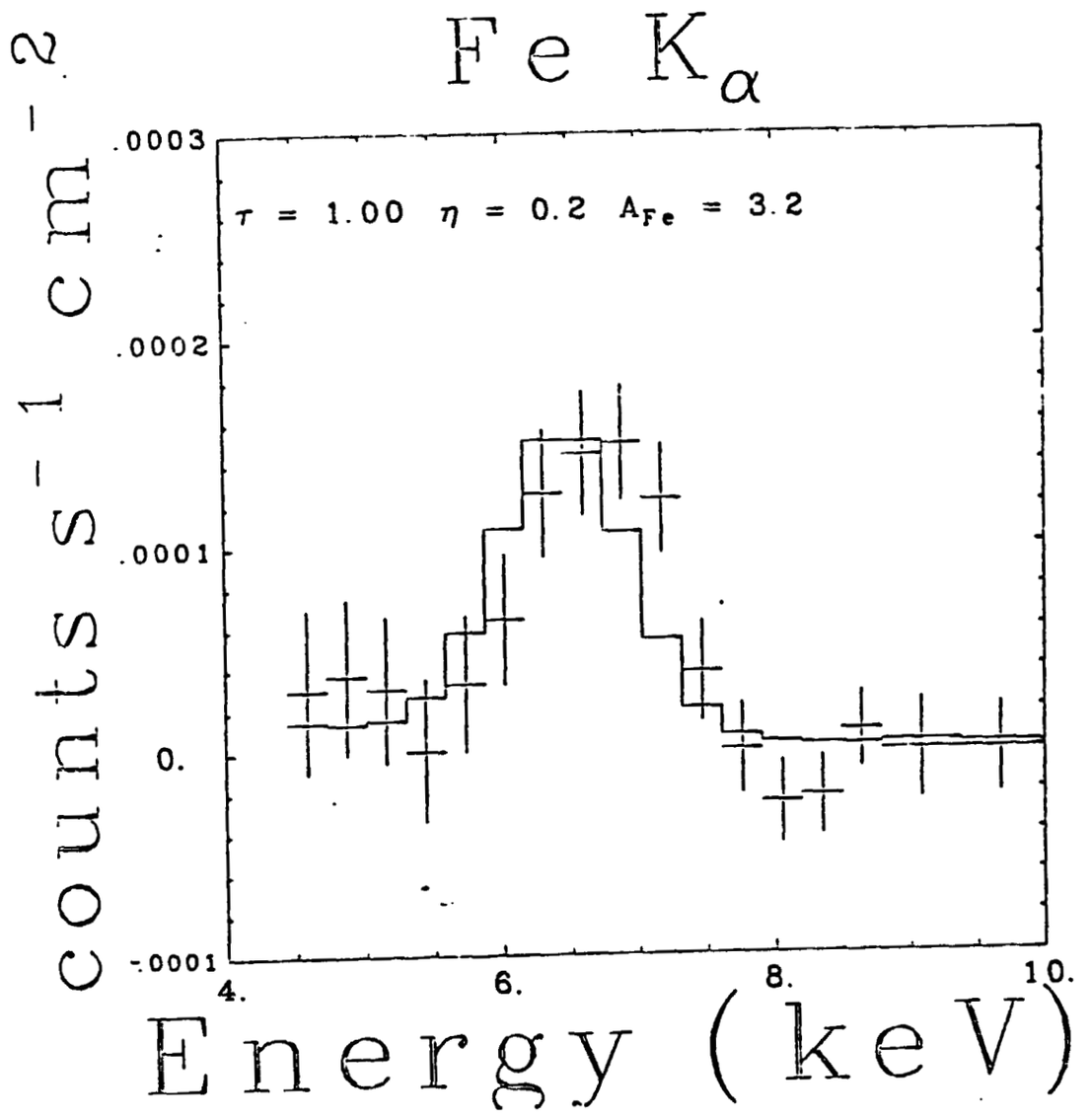

Figure 5a

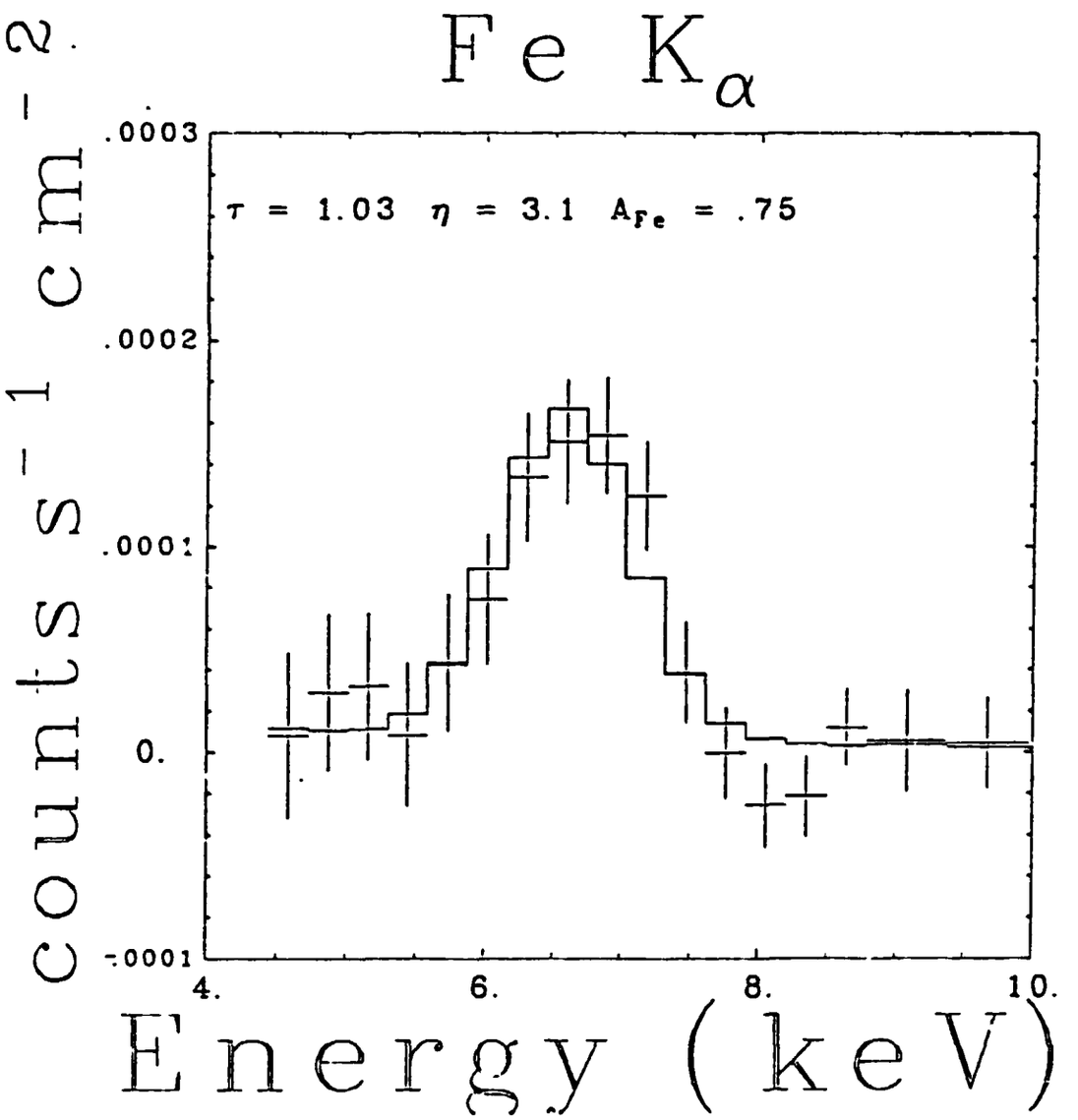

Figure 5b

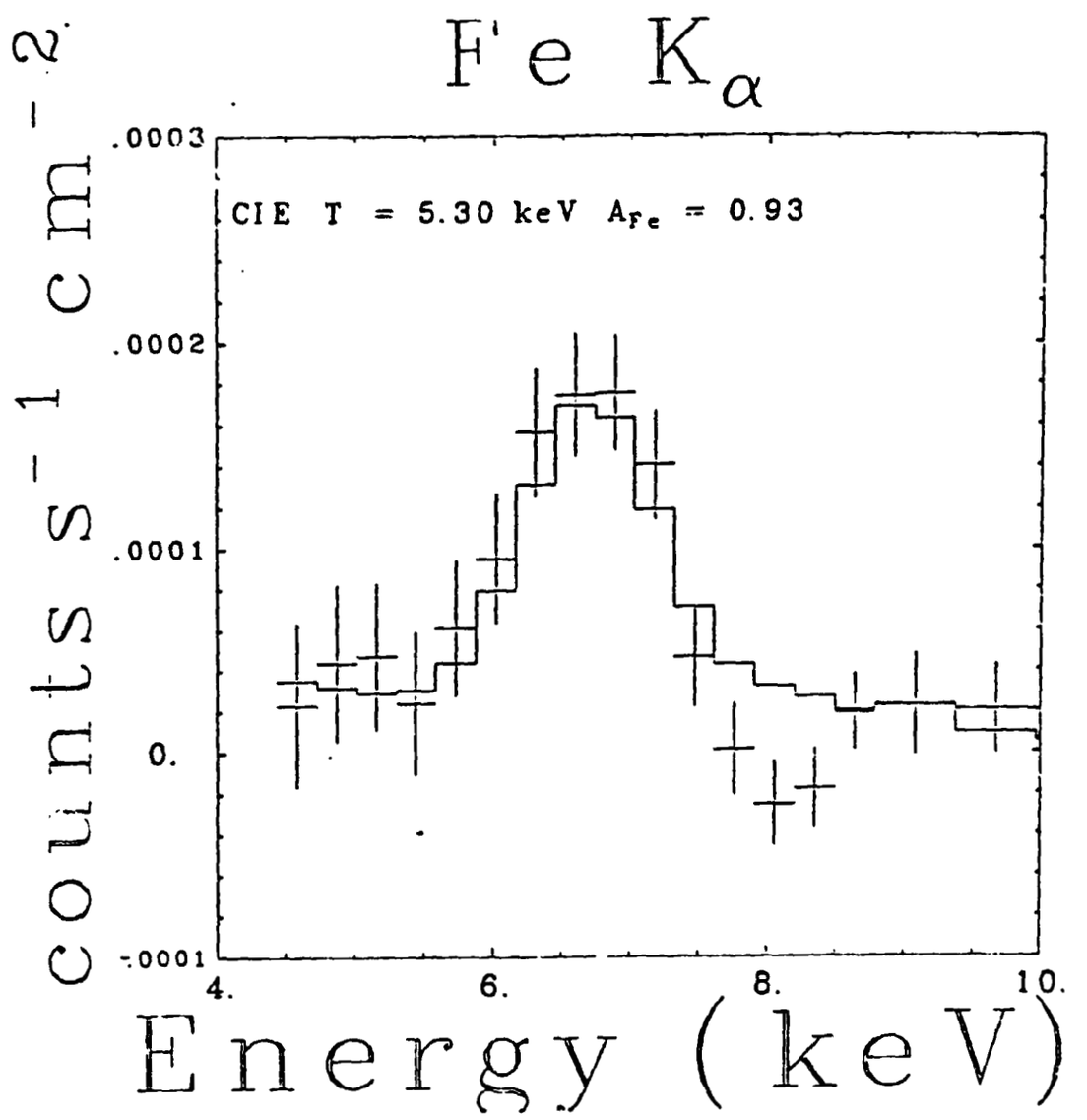

Figure 5c

4.3 The Observation of RCW 103

The first report of x-ray emission from RCW 103 was made by Tuohy et al. (1979) using data from the HEAO A-2 low energy detectors (LED). The detection was made at photon energies $\lesssim$ 3 keV. Fits to the pulse height data using a collisional ionization equilibrium (CIE) plasma model allowed temperatures in the range of $1.3 - 2.0 \times 10^6$ K. Results from the HEAO A-2 medium energy detectors (MED) were ambiguous because of source confusion. An upper limit to the 2 - 10 keV flux was 1×10^{-10} ergs cm^{-2} sec^{-1}. As Tuohy et al. point out, this upper limit does not exclude any temperature that is consistent with the low energy spectral data.

X-ray images have been obtained from the Einstein Observatory. Data from the High Resolution Imaging (HRI) experiment (Tuohy and Garmire, 1980) and the Imaging Proportional Counter (IPC) experiment (Tuohy, private communication) exhibit a limb brightened shell. The surface brightness around the ring is not uniform - the most intense region is in the southeastern part of the remnant. The angular radius of the x-ray emission is $\sim$9 arcminutes. Radio maps of the region also show a ring-like structure of comparable radius (Goss and Shaver, 1970). Optically, filaments exist in the southeast and northwest parts of the remnant. They are contained within a projected radius which is smaller than the radius of the x-ray/radio emission.

An interesting feature of RCW 103 is the presence of a x-ray point source in the geometric center of the remnant (Tuohy and Garmire, 1980). No detectable radio emission has been observed from this point source (Tuohy et al., 1983) suggesting that it may be of a different character from the pulsars that exist at the center of some other supernova remnants (SNR). Tuohy and Garmire suggest that it may be the first detection of thermal radiation from a cooling neutron star.

A distance to RCW 103 of 3.3 kpc is estimated based on the kinematic models of the neutral hydrogen in the spiral arms and absorption profile of RCW 103's

radio continuum at 21 cm (Caswell et al., 1976). This distance estimate along with the measured angular diameter of the x-ray emission would determine the shock radius to be 4.5 pc. This size would indicate that RCW 103 is a young or possibly middle aged SNR. Assuming the kinematics of the shock are described by a Sedov blast wave, the remnant size would imply an age of $\sim 600(n_o/E_{51})^{1/2}$ years, where the particle density of the interstellar medium (ISM), n_o, is in units of 1 cm^{-3}, and the supernova blast energy, E_{51}, is in units of 10^{51} ergs.

Westerlund (1969b) has suggested that the progenitor of RCW 103 might have been a member of an OB association 3.9 kpc away that lies along the line of sight to the remnant. The association with an OB star group would also suggest that the supernova was a Type II event since Type II supernovae are thought to be due to massive, early type stars (e.g. Shklovsky, 1962).

In the previous chapter we presented an analysis of the HEAO A-2 data of SNR, MSH 14-63 (RCW 86), using a model developed to account for non-equilibrium effects in SNR (NIE model). In this chapter we use the model to fit the RCW 103 data collected by the Solid State Spectrometer (SSS) experiment on the Einstein satellite. Because the SSS has good spectral resolution below $\sim$ 4 keV ($\Delta E/E \sim 10\%$), line features can be more readily distinguished with the SSS than with proportional counter detectors flown previously. These line features, each associated with a blend of lines from a single element, are seen prominently in the spectra of most young SNR's. In the SSS, Kα lines from Mg, Si, and S are the three most striking features. Lines from n=3 to n=2 transitions in Fe also produces a large amount of the flux at around 1 keV. To properly infer elemental abundances from the intensities of these features, a proper accounting of the ionic concentrations must be made. Previous work modeling the RCW 103 SSS data have used a CIE plasma model (Becker, private communication). Two plasmas at different temperatures were required to explain the data. In addition, the CIE

model required that the abundances, relative to solar, for the elements of Mg, Si, S, and Fe be $\lesssim 2$. Because the plasma may not be in CIE the calculated ionic concentrations and hence the inferred elemental abundances may be in error. Models which assume non-ionization equilibrium (NIE) in a solar abundance, shock heated, plasma produce a spectrum, that when convolved with a detector response function, can emulate a second, lower temperature component and produce anomalous line strengths relative to a CIE model (Itoh, 1977, 1978, and 1979; Nugent, 1982; Shull, 1982).

The reflection efficiency of the telescope on the HEAO A-2 observatory drops sharply for photons above ~ 4 keV. Consequently no high energy data were obtained with the aforementioned imaging observations (IPC/HRI) or during the SSS observations discussed above. This ignorance of the high energy spectrum has serious consequences for the analysis performed here. Because line emission from heavy elements is the dominant emission mechanism in the part of the spectrum where the SSS is sensitive, interpreting the spectral data requires a complex model; however, above ~ 4 keV the continuum dominates, so measurement of the spectrum at these energies is a less model-dependent measure of the electron temperature and reduced emission volume of the shock heated ISM. Addressing the issue of electron-ion equilibration behind the shock becomes more difficult as result of this lack of data. Measurement of the continuum in this energy range has been definitive in demonstrating that some non-Coulomb electron-ion interactions are present in Cas A (Pravdo and Smith, 1979), Tycho (Pravdo and Smith, 1979), and MSH 14-63 (Nugent et al., 1982).

Despite a growing body of evidence that these non-Coulomb processes exist at the collisionless shock fronts of young supernova remnants, there still does not exist a detailed model of the process, so that we are ignorant of how the magnitude of the effect might vary over a plausible range of SNR shock parameters.

It is known, for example, in the collisionless shocks which occur when the solar wind impinges on the magnetosphere of the earth, that the electron temperature is lower than the ion temperature. Even though we have a bias towards models that have electron-ion equilibration, we will search for evidence of this in the SSS data on RCW 103.

Observations

The spectral data were obtained from observations with the Solid State Spectrometer (SSS) experiment on the HEAO-2 spacecraft. The SSS experiment is described in detail in Joyce et al. (1978). Briefly, the experiment has an effective collecting area of 200 cm^2 and a circular field of view with a diameter of 6 arcmin. Spectral data are collected in the photon energy range from $\sim$ 0.5 to $\sim$ 4 keV.

Because the field of view of the spectrometer is smaller than the angular size the remnant (9 arcmin), a number of different observations are required to obtain the spectrum from the entire remnant. Specifically four observations were performed. Figure 1 is an x-ray surface brightness map showing the positions and approximate extent of the field of view of the different observations. For each of the observations, Table 1 gives the co-ordinates of the center of the field of view, the epoch, and the integration time. The uncertainties in the positions are $\lesssim$ 1 arcmin (Symkowiak, private communication).

Comparison of Observations

The fields of view of the four observations of the RCW 103 remnant do overlap to some extent, but they all sample a different part of the remnant. This gives some limited spatial resolution to the spectra. Before fitting the data we shall statistically test whether the four data sets are consistent with a single, generalized spectral model. By a generalized model, we mean a set of numbers, M_j, where the subscript refers to the jth pulse height channel. Because the surface bright-

ness varies over the remnant and because the amount of the remnant subtended by the field of view during a certain observation varies we will allow the observations to have overall scaling factor, s_i. The subscript in s_i refers to the ith observation.

The X^2 statistic used can be written as

$$X^2 = \sum_{i=1}^{I} \sum_{j=1}^{J} \frac{(s_i M_j - D_{ij})^2}{\sigma_{ij}^2}$$

where D_{ij} is the count rate in the jth pulse height channel of the ith observation, σ_{ij} is the 1σ uncertainty in D_{ij}, J is the number of pulse height channels and I is the number of observations.

The analysis is complicated by a number of effects. First, because certain emitting regions were common to two or more observations, the data sets were not completely independent. For simplicity, though, it was assumed that they were. A second problem concerned the thickness of an absorbing layer of ice that accumulates on the window of the SSS detector. The thickness, hence the amount of absorption of the impinging x-rays varied from one observation to another. The correction of the data for this absorption, in principle, is dependent on the choice of model for the input spectrum. Since no spectrum was assumed for this statistical test, an approximate correction was made by dividing the data for each pulse channel by the absorption factor for photons with energy corresponding to the nominal energy for that channel. A final problem with the data concerns a background component that is known to vary. This problem is most severe in channels which correspond to photon energies $\lesssim$ 2.5 keV. We felt that the shape of the background contamination in these channels is different from the nominal one that has been calculated (private communication, Symkowiak). More attention will be given to this issue later in this paper, but for this comparison here we will ignore the data above 2.5 keV.

The result of the analysis is displayed in Figure 2. The reduced X^2 for the fit was 1.28 for 117 degrees of freedom. The chance of X^2_ν being $\geq$ 1.28 for 117 degrees of freedom if the model were correct is 2.3%. Under the usually criteria of "90% confidence" the model fails the X^2 test and does suggest the possibility of intrinsic differences of the spectrum arising from different regions in the RCW 103 remnant. The slightly high X^2 could be also due to the systematic errors outlined above. Therefore, for simplicity, we will adopt the latter assumption for the remainder of this paper. Given that the spectra are very similar, it isquestionable whether the exercise of modeling each data set separately would produce any meaningful differences.

As was mentioned in the introduction, x-ray images of RCW 103 reveal that there exist surface brightness differences over the surface of the remnant. Because of uncertainties in the precise position of the SSS fields of view and the lack of any detailed data on the x-ray morphology aside from a plot, we cannot confirm that the flux received in the SSS bandpass is consistent with the measured surface brightness with the IPC or HRI detectors. All three instruments have different bandpasses - the SSS being the smallest, so if the SSS and IPC or HRI measurements of the relative surface brightness were inconsistent that would imply that spectral differences outside of the SSS bandpass were responsible for the differences in remnant's x-ray morphology. Alternatively, if that SSS flux is consistent with IPC/HRI result, then variations in the emission integral, $[\int n_e^2 dl]$, would be indicated. Lack of variation in the SSS spectrum implies that the ionization time, $\int n_e dt$, is constant at different positions around the remnant which would further imply that there are no density variations and that variations in filling factors may be responsible for surface brightness variations.

In order to aid future workers on the x-ray morphology of RCW 103, we give the relative de iced flux of the four observations in Table 2. The fluxes are normalized to the flux of observation #1.

Review of Parametcrs

Before discussing results of the model, we briefly review for the reader the definitions of the parameters used. The input parameters to the model and the units we will always use are the initial blast energy, E_o (units of 10^{51} ergs), the density of the interstellar medium around the progenitor star, n_o (units of 1 cm^{-3}), the amount of ejected mass from the progenitor star, M_e (units of $M_\odot$), the age of the remnant, t_3 (units of 1000 years), the abundance, relative to hydrogen, of elements in the ejecta (normalized to the measured solar value), the abundance, relative to hydrogen, of elements in the ISM (normalized to the measured solar value), and the distance to the remnant, D (units of kpc). These parameters are mapped to a more convenient set of parameters for purposes of the doing spectral fitting. There is a scaling parameter defined as

$$\alpha = \left(\frac{E_o}{n_o} \right)^{1/3}$$

and a number of "reduced" parameters:

$$\eta = (E_o n_o^{\ 2})^{1/3} = \alpha^{-2} E_o = \alpha n_o \ ,$$

$$\beta = \frac{M_e}{E_o} = \eta^{-1} \alpha^{-2} M_e \ ,$$

and

$$\tau = \left(\frac{n_o}{E_o} \right)^{1/3} t_3 = \alpha^{-1} t_3 \ .$$

A fourth reduced parameter is the reduced emission volume, C_{ev}, which is defined as

$$C_{ev} \equiv \frac{\int n_e^2 dV}{4\pi D^2} \quad .$$

η, τ, β, and C_{ev} are derived from fits to the spectral data. α is then determined from the average x-ray surface brightness by

$$\alpha = \frac{\Sigma'(\eta,\beta,\tau)\theta^2}{C_{ev}} f$$

where Σ' is determined from η, β, and τ and f is the fraction of solid angle of the remnant filled by shocked plasma. The value of f will nominally be asumed to have a value of unity. With α, the input parameters are given by

$$E_o = \alpha^2\eta \quad M_e = \alpha^2\eta\beta \quad t_3 = \alpha\tau \quad n_o = \alpha^{-1}\eta$$

and the distance is given by

$$D = \frac{R_s'(\beta,\tau)\alpha}{\theta} \quad ,$$

where R_s' is a constant determined from the fitted value of β and τ.

When $\tau \gtrsim 16\beta^{5/6}$ the remnant is in a Sedov phase and the shock temperature, T_s, can be given as a function of τ by

$$T_s = 3.2\ \tau^{-6/5}\ \text{keV} \quad .$$

Fits to Spectral Models

As was discussed in the section concerning comparison of observations, there are systematic problems with the background data above 3.0 keV. In the case of the RCW 103 data there were problems reconciling the data with the fitting models

at photon energies $\gtrsim$ 2.5 keV. We will first present results, considering fits to the data below 2.5 keV and then discuss the residuals above 2.5 keV.

We will first discuss models similar to those used by Hamilton et al. (1982). As discussed above these models use Sedov hydrogynamics and are equivalent to this model only in the "far Sedov" limit ($\tau >> \tau_s$). The models were fit with β fixed at 2 (β must be finite for numerical reasons.) and no ejecta emission was considered. Models where the ejecta were included are discussed below. The results of the fit with the "hot" electron ($T_e = T_m$) model are given in Table 3 and the dtat with the model are shown in Figure 3b. Likewise, the "cold" electron ($T_e \neq T_i$) model results are given in Table 3 and the data with the model are displayed in Figure 3a. For both of these fits $\tau/\tau_s \gtrsim 12$, thus assuring our desire to be in a "far Sedov" limit. The parameters that were varied were C_{ev}, n, τ, N_H, and the abundances for magnesium (A_{Mg}), silicon (A_{Si}), sulphur (A_s), and iron (A_{Fe}). The rest of the elemental abundances were fixed at their solar value.

On the assumption that the emission is from a uniform ISM shocked by a Sedov blast wave, we have inferred the input parameters by the method described in the last section. In addition to the filling factor, f, there is a related effect that the SSS field of view is smaller (6 arcminute) than the extent of RCW 103 (9 arcminute), and, thus the measured C_{ev} given in the tables is an underestimate. Most of the exposure of the data comes from observations 3 and 4 where the remnant filled the entire field of view, so, as an approximation, we corrected C_{ev} before calculating α by the ratio of the solid angle of the remnant to the solid angle of the SSS beam. We took that ratio to be $\sim$2. The value for α and the inferred input parameters are given in Table 3.

The fits to the data are not of high quality. The reduced X^2 obtained would result < 0.1% by chance. It is possible that the high X^2 are in part due to improper modeling of detector output to a given input spectrum indlucing back-

ground effects, but, even if all the problems were due to detector modeling as opposed to source modeling, there is no reason to believe that our best fit parameters are close (compared to the statistical uncertainties) to the best fit values given ideal detector modeling. Despite this caveat, we performed on the "hot" electron model a contraction of X^2 space onto the η-τ plane. Every point on this plane represents the best fit X^2 if η and τ are fixed at the values given at that point and all others are allowed to vary. The results are shown in the insert of Figure 3b. Two contours are given. The first is for values of X^2 which exceed the minimum X^2 by 4.6. This corresponds to 90% confidence region for 2 interesting parameters (Lampton et al., 1976). Another contour at $\Delta X^2 = 10$ is given. Two representative points near the extremes of his region are also shown in Table 3. These illustrate rough statistical limits for the various parameters.

We note that the "valley" of X^2 on the η-τ plane roughly runs along a line of constant effective ionization $\eta\tau$. The fits are snesitive to the shape of the Kα lines of the principal elements. Each Kα blend is composed of emission from the hydrogen-like ion, helium-like ion, lithium-like ion, etc. Each ion emits at slightly different energies that are roughly ordered by the ionic charge. The SSS does not, of course have the capability to resolve these blands of lines, but they can be inferred from the shape and centroid of the line which, assuming kT_e is much greater than the energy spacing, will be dependent on the relative concentration of the ionic species. These ionic concentrations depend somewhat on the temperature history, but for the temperatures and elements of interest here, the ionic structure is a more sensitive function of $\int n_e dt$. This is the reason that X^2 contours remain close to iso-$\eta\tau$ contours.

We will first discuss the significance of the different parameters individually. Following that, we will make some general comments and summarize the main points.

Contribution from the ejecta

The possibility of an ejecta emission component resulting from a "reverse" shock wave has been discussed by McKee (1974) and Gull (1973, 1975). As has been discussed this reverse shock component manifests itself in one-dimensional hydrodynamic codes like the one used in this model, so, in principle, we can use our NIE to search for the evidence of this component in the x-ray spectral data.

When reverse shock emission from the ejecta was included in the model, best X^2 were obtained when the ejecta did not contribute significantly to the measured flux. Either the ejecta had a small fraction f the emission volume or the ejecta component had a temperature $\lesssim$ 100 ev-a temperature to which the SSS is insensitive. It is possible, however, to find models that do have a significant ejecta component that are not in gross disagreement with the data. To demonstrate this a search was made in a restricted part of parameter space for which $\tau < 4\tau_s$. β was allowed to vary, along with the parameters mentioned above. Our spatial and spectral resolution were not sufficient to deconvolve the ejecta contribution to line strengths from the ISM contribution. Hence the abundance parameter for a given element in the ejecta and the abundance parameter for the same element in the ISM are highly correlated in the fitting process. One can be arbitrarily decreased and, to compensate, the other can be increased without significantly changing X^2. This problem can be avoided by fixing one of the abundance sets. In most modeling runs the contribution of the ejecta turned out to be a smaller fraction of the emission, so the ejecta was chosen to be the fixed set. Solar abundances for the ejecta were used; however, this might be a poor choice, especially if the progenitor was a Type II supernova.

The results of this search for "hot" and "cold" electron models are shown in Table 5 and Figure 4. In the case of the "cold" electron model a local minimum X^2 in parameter space was found, but for a "hot" electron model τ needed to be

constrained in order to satisfy the condition of being $< 4\tau_s$. Both fits give somewhat worse but comparable X^2 to models where the ejecta was ignored.

Electron heating at shock fronts

The issue of whether electrons are heated by non-Coulomb processes in the chock of RCW 103 is not clearly resolved by the fits to the SSS data. One reason, mentioned before, for this ambiguity is the inability to directly measure the high energy continuum which gives a relatively model-independent measure of the electron temperature. That inability is related to the insensitivity of the SSS to photons with energies $\gtrsim$ 4 keV and is a general problem when relying solely on data from the SSS experiment. Assuming the results of the NIE model are roughly correct there is a more fundamental problem, intrinsic to the RCW 103 SNR. RCW 103 is apparently in a part of η-β-τ space where the "cold" and "hot" models are beginning to become indistinguishable. The age, t_{eq}, at which the electron temperatures predicted by a "cold" electron model and a "hot" electron model begin to become indistinguishable is given by Cox and Anderson (1982) as

$$t_{eq} = 3000\ E_{51}^{3/14}\ n_o^{-4/7}\ \text{years}$$

where E_{51} is the balst energy in units of 10^{51} ergs and n_o is the ISM particle density in units of cm^{-3}. The ratio of the age, t, to t_{eq} is independent of α and, in terms of our parameters, is given by

$$\frac{t}{t_{eq}} = \frac{\tau}{3}\,\eta^{5/14} \quad .$$

For $\eta = 0.5$ and $\tau = 3.6$, $t/t_{eq} = 0.94$. The fact that the best fit points for both models lie roughly in the same region of parameter space is consistent with the

fact that the models a. . beginning to converge in that region. For $t >> t_{eq}$ the differences in the two model spectra become negligible, but at $t \sim t_{eq}$ only the differences in the predicted electron temperature and hance the continuum spectra becomes negligible. The fact that the fits are not completely similar can be explained by the different electron temperature histories of the shock gas. In the "hot" electron model, the electron temperature of a particular gas element has been decreasing monotonically ever since that gas element has been shocked, while during some or all of that time the "cold" electron model predicts that the temperature has been increasing. Since the evolution of the ionization structure is dependent on the evolution of the electron temperature, it is reasonable to expect differences between the two best fit points in parameter space, particularly the elemental abundances.

Elemental abundances

The fitted ISM elemental abundances in the "hot" electron model are consistent with a solar set. This differs from the results using CIE models by Becker (private communication). The abundances required by the CIE models are a factor of 2-3 (Table 5) higher relative to solar. The abundances determined by the "cold" electron model deviate from solar by up to factor of ~ 4.

Since a solar abundance set is nominally expected from a interstellar gas, the results of the NIE "hot" electron model are pleasing. The abundance results may be closer to solar than are shown in Table 3. For historical reasons an Allen (1976) abundance set was used. More recent work by Meyer (1979) shows some significant deviations from Allen for some elements. The conversion between to the two abundance sets is complicated by the fact that the continuum flux is dependent on the elemental abundances, particularly C, N, and O; however, as an approximation we will correct each element by its ratio in the two abundance

sets. With that correction, the best fit abundances for Mg, Si, and Fe are all within 5% of solar. This makes the Meyer solar value consistent for each of these elements. The only statistically significant deviation is for S which has Meyer abundance of 1.2.

Not all results from applying NIE models to SSS data of young SNR's have demonstrated solar abundances. Work on Tycho's SNR (Shull, 1982), for example, has shown overabundances still are predicted by NIE models. The distinction may result from the dominance of the role played by the ejecta in the x-ray emission, since the ejecta is thought to be metal rich. In addition to the emission from the ejecta following heating from a reverse shock, ejecta may also mix with hot ISM and heat by conduction.

Distance, density, and interstellar absorption

The distance measurement is consistent with the 3.3 kpc estimate made by Caswell (1976). It also is consistent with the distance measured to Westerlund's OB star group, strengthening the argument for association of the progenitor of RCW 103 with that group.

The height of RCW 103 off of the galactic plane is 23 pc assuming a distance of 3.3 kpc. The inferred particle density of ~ 1 cm^{-3} is reasonable for that position.

Finally, assuming a distance of 3.3 kpc, the measure of N_H, would imply a mean density of ~ 0.4 cm^{-3} in the intervening ISM. Again, this is a reasonable value.

Age

The age of RCW 103 has consequences for the issue of the lack of historical record of the supernova which formed RCW 103 and of the cooling of central point source seen by Tuohy and Garmire (1979). We will adopt for this discussion the

age, with uncertainties, determined from the "hot" electron model. First, to put this work in perspective, we note that limits can be put on the age of RCW 103 without resorting to the use of the elaborate NIE model. Taking the radius of the remnant to be 4-5 pc and assuming that the average velocity of the ejected material is $\lesssim$ 0.1 c would put a lower limit to the age of $\sim$ 140 years. From crude spectral modeling of x-ray data a lower limit for the shock temperature can be determined to be $\sim$ 0.2 keV. That limit on the temperature along with the measurement of the size of the remnant can be used to assert an upper limit to the age of $\sim$ 6000 years.

Due to its apparently young age and close proximity to the sun, RCW 103 could be expected to be a historical supernova. As pointed out by Clark and Stephenson (1976) if RCW 103 is younger than 600 years the initial supernova event could have escaped attention by Chinese astronomers, since the capital of China was at Peking for most of the time after AD1280. Peking is too far north (latitude $\sim$ +40) to able to see RCW 103. Chinese records become more scarce before $\sim$ 200 BC, so, if the age of RCW 103 is $\gtrsim$ 2200 years, the non-detection of its supernova, could again be explained. At intermediate times, records existed, the capital was farther south, and the effect of the earth's precession made objects in the direction of RCW 103 more visible in northern latitudes. From the NIE model, RCW 103 is most likely of this intermediate age. To emphasize the point that the Chinese were able to monitor objects in the direction of RCW 103, they did record supernovae in AD 185 at $\alpha \gtrsim 15^h$, $\delta \gtrsim -62°$ (1950) and in AD 393 at $\alpha \gtrsim 17^h$, $\delta \gtrsim -40°$ (1950). They should have had an unobstructed view of the RCW 103 supernova, which is at $\alpha \gtrsim 16^h$, $\delta \gtrsim -51°$ (1950), if the event took place at the time determined by the NIE model.

As also pointed out by Clark and Stephenson (1976) even if the RCW 103 supernova took place during a time when Chinese could observe it, the likelihood

of detection could still have been reduced if RCW 103 was near conjunction with the sun at the time of the event. We also point out that Cas A, which is thought to be at the same distance as RCW 103, most likely escaped detection as a historical supernova. If anything, Cas A was a more likely candidate for detection since it was probably more recent and definitely at a much more favorable declination for viewing in the northern hemisphere.

A second issue related to the age of RCW 103 is the cooling rate of the point source in the center of the remnant. Under the assumption that the object is a neutron star and that no mechanism exists for renewing the internal energy of the core, then knowing the age of the neutron star could be a test for different suggested cooling mechanisms (Bahcall and Wolf, 1965; Glen and Sutherland, 1980; Normoto and Tsuruta, 1981; Richardson et al., 1982). The NIE model can only be an effective discriminate of cooling mechanisms if the cooling time scale is within this allowed range for the age of RCW 103. This probably is not the case. Neutrino cooling following pion beta-decay is the fastest cooling mechanism with cooling time scales $\sim$ 1 year. This can be easily ruled out for RCW 103's neutron star. Recent calculations by Richardson et al. which do not assume a pion concentrate in the core give cooling curves that are consistent with the age measured here and the effective temperature of 2.2×10^6 K measured by Tuohy and Garmire. In principle, the age and effective temperature could be used within the framework of models - such as Richardson et al. - to determine the mass of the neutron star; however, the uncertainties in the measured quantities were too large to allow this.

Blast Energy

The value determined for the blast energy, $\sim 6 \times 10^{50}$ ergs, is somewhat low compared to the numbers that are usually associated with supernova blasts

($\sim$0.4 - 4 x 10^{51} ergs). Some care must be taken before accepting this upper limit, however. Because the inferred value of the blast energy scales like η^5, it would only take an increase of $\sim$ 10% in the fitted upper limit of η to account for the discrepancy.

Since Type I supernovae are thought to have lower blast energies ($E_{51} \lesssim 0.5$) then to Type II ($E_{51} \lesssim 1$), the low fitted value of E_o would be weak evidence for the progenitor of RCW 103 being a Type I supernova.

Summary

Our inability to settle the question of electron-ion equilibration at the shock front may be due, as suggested, to intrinsic properties of the RCW 103 remnant; however, this ambiguity and the ambiguity on the question of reverse shocked ejecta are exacerbated by poor knowledge of the spectrum above 2.5 keV. This part of the spectrum is dominated by continuum emission and as a result gives a measure of the electron temperature independent of many of the systematic problems of the NIE model. It also gives a direct measure of the reduced emission measure of this high temperature component which provides a baseline for interpreting the "excess" of flux at 1-2 keV. As can be seen from the analysis of the RCW 86 data, this information constrains the permitted volume of parameter space severely even without detailed knowledge of the line emission.

Knowledge of this component could, for instance, help to distinguish between "cold" and "hot" electron models. The "hot" model would predict a shock temperature of $\sim$ 1-2 keV and reduced emission volume of $\sim$ 1 x 10^{13} cm^{-5} while the "cold" model would have the high temperature be $\sim$ 0.7 keV and the reduced emission volume be $\sim$ 3 x 10^{13} cm^{-5}.

An important future observation will be the determination of the behavior of the spectrum at photon energies above 2.5 keV. Source confusion has thwarted efforts to do so with HEAO-1 and the high energy cutoff of the x-ray mirrors on HEAO-2 prevented the SSS from operating in that region. AXAF, BBXRT, as well as

more modest shuttle and Explorer missions should have the capability to make this measurement.

Despite the poor coverage of the spectrum, the SSS data on RCW 103 does, of course, provide a good opportunity to study the intensity of the line emission and, hence, deduce elemental abundances. On this note we consider the NIE model to have been a success. Assuming the "hot" electron model is correct, the data do support the idea that the x-ray emission is arising from shocked ISM with elemental abundances roughly the same as solar. The 'hot' electron model is preferred because the "cold" electron model has been ruled out in other yound SNR's.

Finally, we note that there are indications that RCW 103 may have up to four unique or almost unique characteristics relative to other young SNR's. With parenthetical comment, these are:

1) The radio surface brightness is low by factor of 5-10 from other remnants of comparable diameter (This is fairly certain; Clark and Caswell, 1976).
2) A low value of the blast energy E_o is derived here. (Many assumptions used.)
3) The supernova was not detected. This possibly suggests a low peak optical luminosity for the supernova. (Other plausible reasons exist.) This argues for a Type II supernova which is inconsistent with feature number 2.
4) A central point source exists that is not a radio pulsar. (This is fairly certain.)

How many of these are true anomalies and what possible connection exists between them is an open question.

Data > 2.5 keV

Figure 5 shows all the data displayed with the $T_e = T_m$ model given in Table 3. The model underestimates the data at photon energies $\gtrsim$ 2.5 keV. We will restrict our discussion to the electron-ion equilibrium model since the "cold electron"

model gives similar results in this energy range. The possibility exists that this anomaly is caused by an incorrect measurement of the background. The background of the SSS is knwon to have two components (Symkowiak, private communication): a "constant" background component that is simply proportional to the integration time of the observation and a "bump" background component that is also nominally proportional to the integration time but also has a scale factor relative to the constant background that can vary from one integration to another. I is customary to allow this scale factor to be a fitting parameter.

Figure 6 shows the residuals at the end of the spectrum for observations 1, 2, 3, and 4, respectively. The model used was the same one used to the fit the composite spectrum. The only variable in the input model between the different fits was the overall normalization factor which was determined only by the data with photon energies < 2.5 keV. The "bump background" scale factor was also a free parameter. Figure 5b displays the bump background component. The bump background alone cannot account for all the anomalous residuals. As can be seen, the shape of the anomalous residuals is different from the bump background component. In some cases the residuals have a maximum value at $\sim$ 2.7 keV where the bump background is very small compared to its peak value.

The inability of the standard background subtraction procedure to account for the anomalous residuals does not preclude the possibility that the problem is related to background subtraction. Other variations in the intensity and spectrum from the nominal background model are suspected in other SSS observations (Symkowiak, private communication). Most of the background is produced by false counts made by charged particles in the magnetosphere of the earth. Variations in the density and spectrum of these charged particles can explain variations in the SSS background. Indeed, the "bump" background scheme was an empirical attempt to account for these variations but perhaps not comprehensive enough.

Table 6 gives a measure of the residuals in each of the observations. The residuals were averaged between the energy of 2.5 and 3.2 keV. This range was chosen to minimize the dependence of measurement on the amount of "bump" background. Also given, for comparison, is the average flux over the range of 0.8 to 2.5 keV received during the various observations. The residuals from observations 1 and 2 are twice as large as observations 3 and 4. This may be significant since the first two observations form a distinct set, grouped in time, from the last two observations. As can be seen in Table 1, observations 1 and 2 and observations 3 and 4 were close together in time but, the epochs for each pair were relatively far apart ($\sim$ 9 days). The observations in the first pair looked at edges of the remnant and subtended a smaller fraction of the surface brightness than the second pair which was more centrally located on the remnant. The count rates from the first pair were smaller for this reason. The first pair also has shorter integration times. The correlation of the intensity of the residuals with the epoch of the observation and the anti-correlation with the intensity of the known source intensity at other photon energies would support the notion that the residuals were caused by an inaccurate model of the background. Anti-correlation of the residual intensity with integration time might also be indicative of background problems. Examination of other observations taken during this time have not been helpful. The source intensity at the pertinent energies overwhelmed the effect we were looking for in other observations. In any case, the effect might vary with position over the earth as well as the orientation of the telescope relative to the direction of the magnetic field and both of these parameters may be correlated with the pointing of the telescope in the direction of RCW 103. However, the evidence for background contamination is far from conclusive, and we now examine possible contributions to these residuals that originate at the remnant.

Attempting to explain the residuals in terms of emission from an optically thin plasma is difficult. The data require a rising photon spectrum at photon energies greater than 2.5 keV. Any additional continuum component, then, falls off faster than the data regardless of the temperature. Line emission is a possible explanation, but it has difficulties. Any significant contribution due to the line emission from elements with ($Z \leq 16$) can be ruled out. The strength of the Kα emission features gives upper limits to the amount of power from these elements in the lines above 2.5 keV. For example, one of the most powerful lines of this type is a result of an $n = 3$ to $n = 1$ transition in S XV (line energy at 2.88 keV). Even under the most optimistic condition the power in the S Kα feature would constrain the power in the 2.88 keV line to be factor ~ 7 below that required to explain the data at that energy. An overabundance of chlorine of a few hundred relative to solar could explain the data but is unlikely.

Before considering other spectral forms, a relevant factor is the central point source of the remnant. Enough systematic uncertainty exists that it cannot be said for sure whether or not the point source was within the field of view of the detector during each observation. It was certainly within the field of view during observation number 4 and most likely within the field during observation number 3. Given the nominal positions, the point source was not involved in observations number 1 and 2. Including possible offsets of the collimator (Symkowiak, private communication), it might be in one of those fields of view, but not both of them. It is not possible, then, for the point source to explain all the residuals. It is possible that the residuals in observations 1 and 2 are not caused by the same phenomenon as in latter observations, so we cannot rule out the role of the point source in this matter.

A black body spectrum required a temperature of ~ 5 keV and an emitting region with a characteristic size of ~ 100 m at a distance of 4 kpc. Taking a neutron star density as an upper limit to the density of the emitting region, we calculate that the cooling time for this proposed black body would $\lesssim 100$ days. Thus the

emitting region would need to be $\sim$ 0.01 the size of a neutron star and would need to be re-energized.

Conclusions

The main conclusions of this chapter are:

1) No variation can be detected in the spectrum collected from different regions of the remnant.
2) The data cannot be used to discriminate between whether non-Boulomb electron-ion energy excahnge processes may be present at the shock front.
3) Assuming that non-Boulomb processes are present - a likely hypothesis given results from other young SNR's, the data are consistent with the idea that the emission is all from the shocked interstellar medium with approximately solar composition of heavy elements.

Table 1

RCW 103 Observation Record

Obs #	<Obs. time> (Day of 1977)	Int. time (s)	Position R.A. (1950)	Dec. (1950)
1	425.611	1679.4	243.500	-50.967
2	425.378	1638.4	243.343	-50.899
3	434.122	3604.5	243.425	-50.933
4	434.663	4341.8	243.458	-50.883

Table 2

Relative de-iced fluxes

Obs #	Relative Flux
1	1
2	0.858 ± 0.035
3	1.424 ± 0.045
4	1.351 ± 0.044

Table 3

NIE Model without ejecta

	$T_e \neq T_i$	$T_e = T_i$		
	best fit	best fit	~ limits	
C_{sv} (10^{13} cm^{-3})	1.8	0.56	0.66	0.35
η (foe$^{1/3}$ cm^{-2})	0.5	0.34	0.30	0.49
β ($M_\odot$ foe^{-1})	-	-	-	-
τ (kiloyears cm^{-1} foe$^{-1/3}$)	3.6	4.2	4.8	3.0
N_H (10^{21} cm^{-2})	5.0	3.7	4.1	3.2
A_{Mg} (solar)	0.83	1.5	1.4	2.1
A_{Si} (solar)	0.79	1.0	1.0	1.2
A_S (solar)	1.9	1.3	1.6	1.3
A_{Fe} (solar)	0.20	0.75	0.71	1.3
χ^2_ν ($\nu = 31$)	2.3	1.9	2.1	2.1
α (foe$^{1/3}$ cm)	0.23	0.37	0.26	01.1
E_0 (foe)	0.03	0.05	0.02	0.6
n_0 (cm^{-3})	2.1	0.92	1.2	0.45
t_g (10^9 years)	0.85	1.6	1.2	3.2
D (kpc)	1.6	2.6	1.9	6.7

cb. foe $\equiv 10^{51}$ ergs (fifty-one ergs; © Hans Bethe)

Table 4 Two Temperature CIE Model	
$C_{ev,low}$	1.1×10^{13} cm^{-5}
$T_{e,low}$	0.51 keV
$C_{ev,high}$	8.4×10^{11} cm^{-5}
$T_{e,high}$	$\gtrsim$6 keV
N_H	5.9×10^{21} cm^{-2}
A_{Mg}	2.3 solar
A_{Si}	1.9 solar
A_S	3.2 solar
A_{Fe}	2.9 solar

Table 5

NIE Model with ejecta

	$T_e \neq T_i$	$T_e = T_i$
C_{ev} (10^{13} cm^{-3})	2.0	0.31
η (foe$^{1/3}$ cm^{-2})	0.64	0.55
β ($M_\odot$ foe^{-1})	4.9	3.0
τ (kiloyear cm^{-1} foe$^{-1/3}$)	1.6	> 1.6
N_H (cm^{-2})	4.7	0.29
A_{Mg} (solar)	1.1	3.1
A_{Si} (solar)	0.83	1.4
A_S (solar)	1.2	1.2
A_{Fe} (solar)	0.2	2.4
χ^2_ν (ν = 30)	2.7	2.6
α (foe$^{1/3}$ cm)	0.45	> 1.7
E_0 (foe)	0.13	> 1.6
M_e ($M_\odot$)	0.6	> 4.8
n_0 (cm^{-3})	1.4	< 0.32
t_3 (10^3 years)	0.72	> 2.7
D (kpc)	2.4	> 9.2

Table 6

Obs #	Residual flux (2.5 - 3.2 keV)	Total flux (0.8 - 2.5 keV)
1	4.5 ± 0.9	26.5 ± 0.9
2	4.7 ± 0.9	28.6 ± 1.0
3	2.1 ± 0.6	49.3 ± 0.8
4	2.3 ± 0.5	38.1 ± 0.7
	10^{-2} cnts (SSS area)$^{-1}$ s^{-1} keV^{-1}	

Figure Captions

Figure 1

The x-ray surface brightness map (Touhy, private communication) from the Imaging Proportional Counter (IPC) experiment on the HEAO A-2 spacecraft. Circles represent the four fields view of the SSS observations.

Figure 2

The results of attempting to find a generalized model that was consistent with the four different observations are displayed. Histogram represents model.

Figure 3

Results are shown of best fits to the data when no ejecta was included (far Sedov limit). (a) is for Coulomb heating model and (b) assumes electron-ion thermal equilibrium. Insert in (b) is the projection of X^2 space on the $\eta - \tau$ plane. Contours show the change of X^2 from the best fit. Both 4.6 and 10 are shown.

Figure 4

Results are shown of best fits to the data when ejecta was included. (a) is for Coulomb heating model and (b) assumes electron-ion thermal equilibrium.

Figure 5

Figure 5 shows the same fit as was in Figure 3b but, now, all the data is shown. (b) displays the residuals of the fit and (c) gives the bump fraction function for comparison.

Figure 6

The residuals from each observations to the model in Figure 3b are shown.

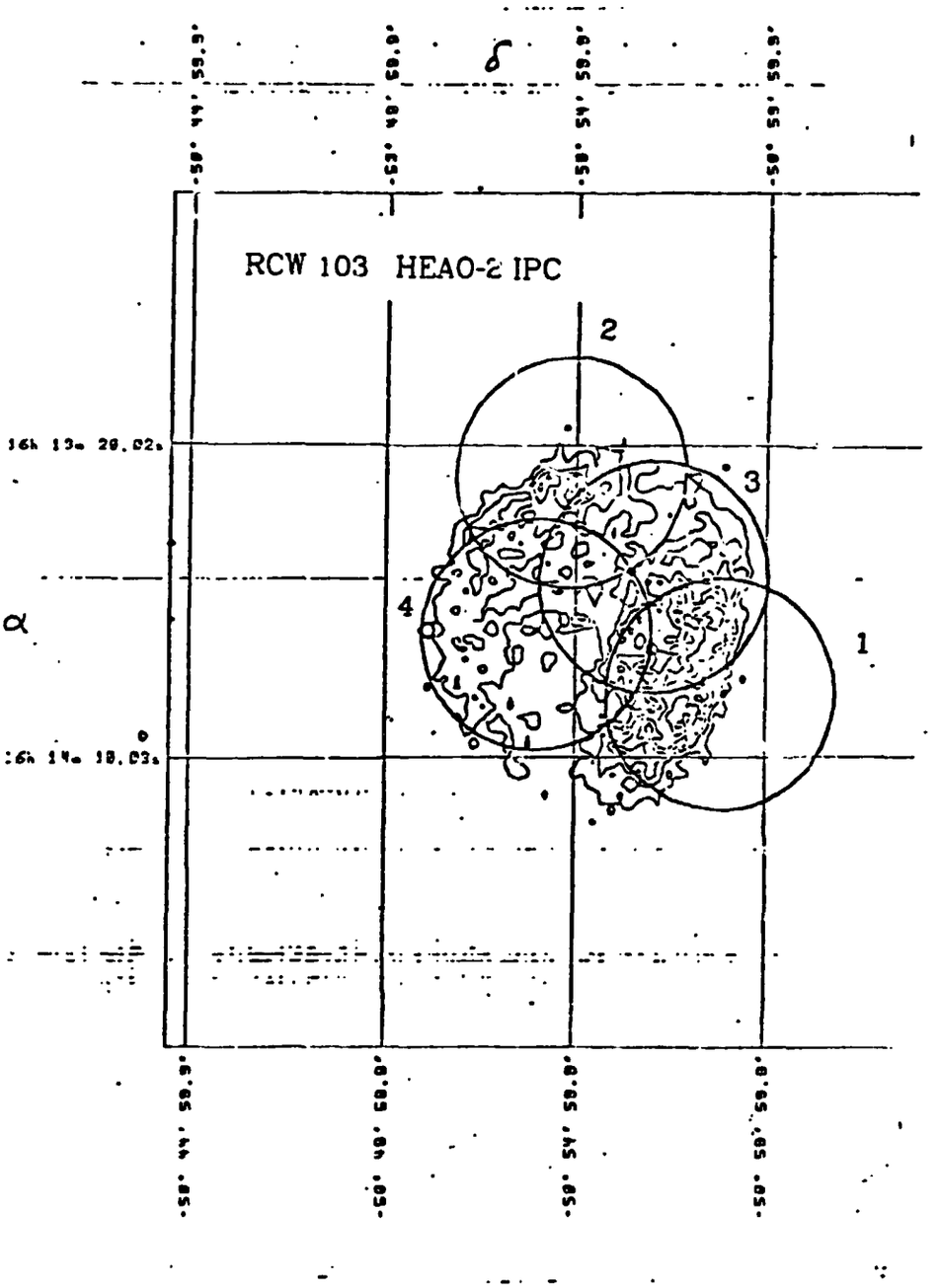

Figure 1

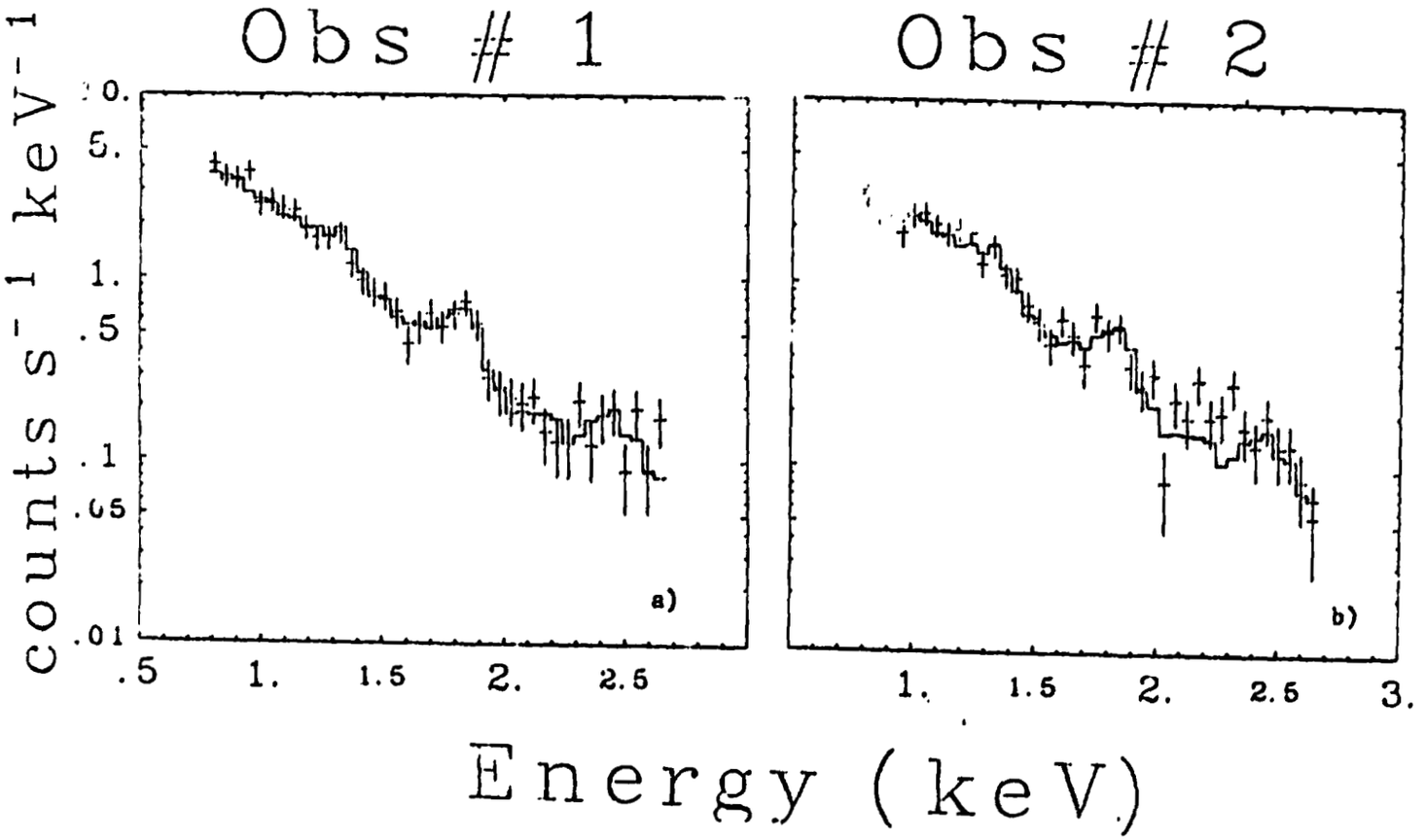

Figure 2

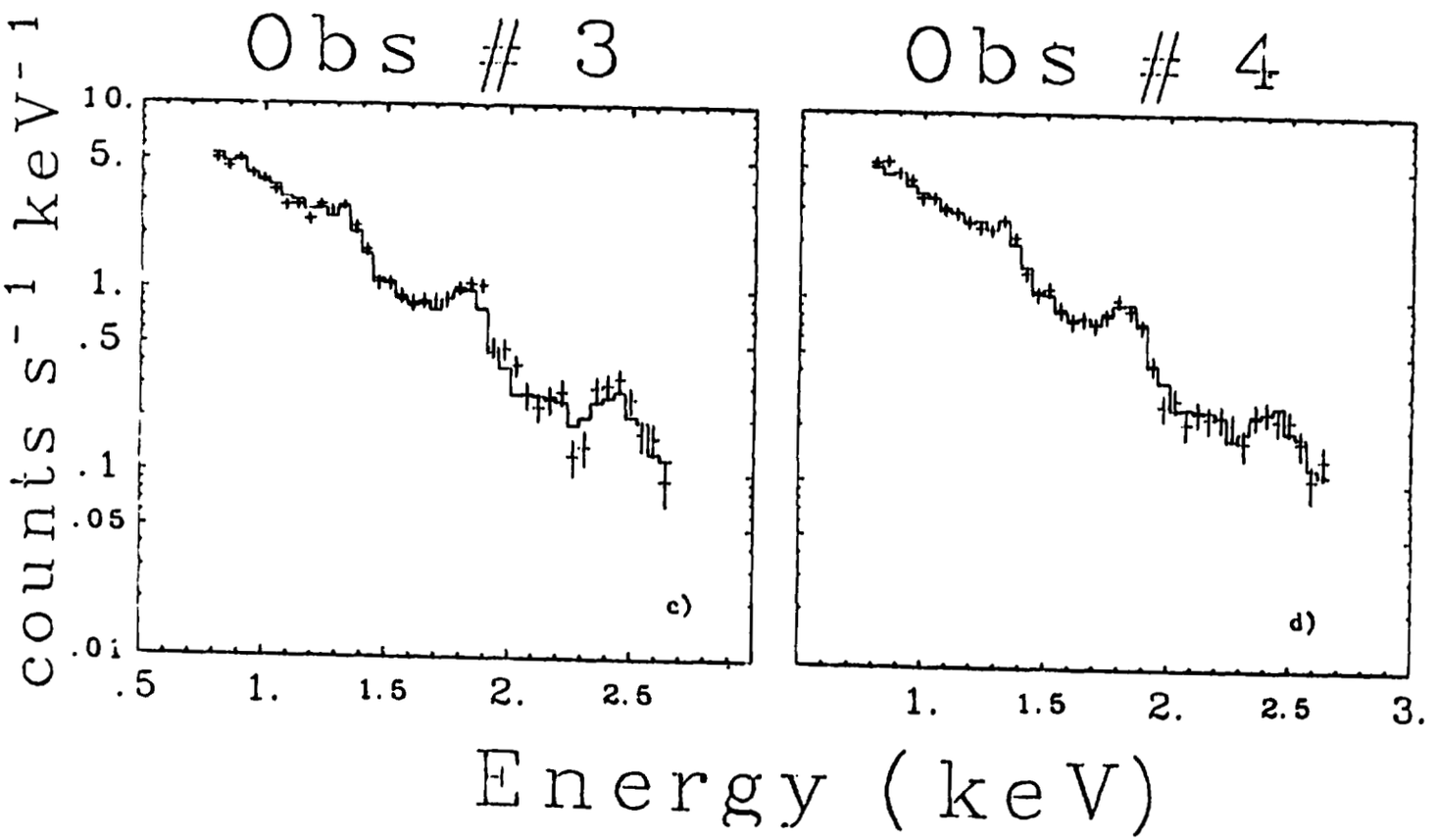

Figure 2 A

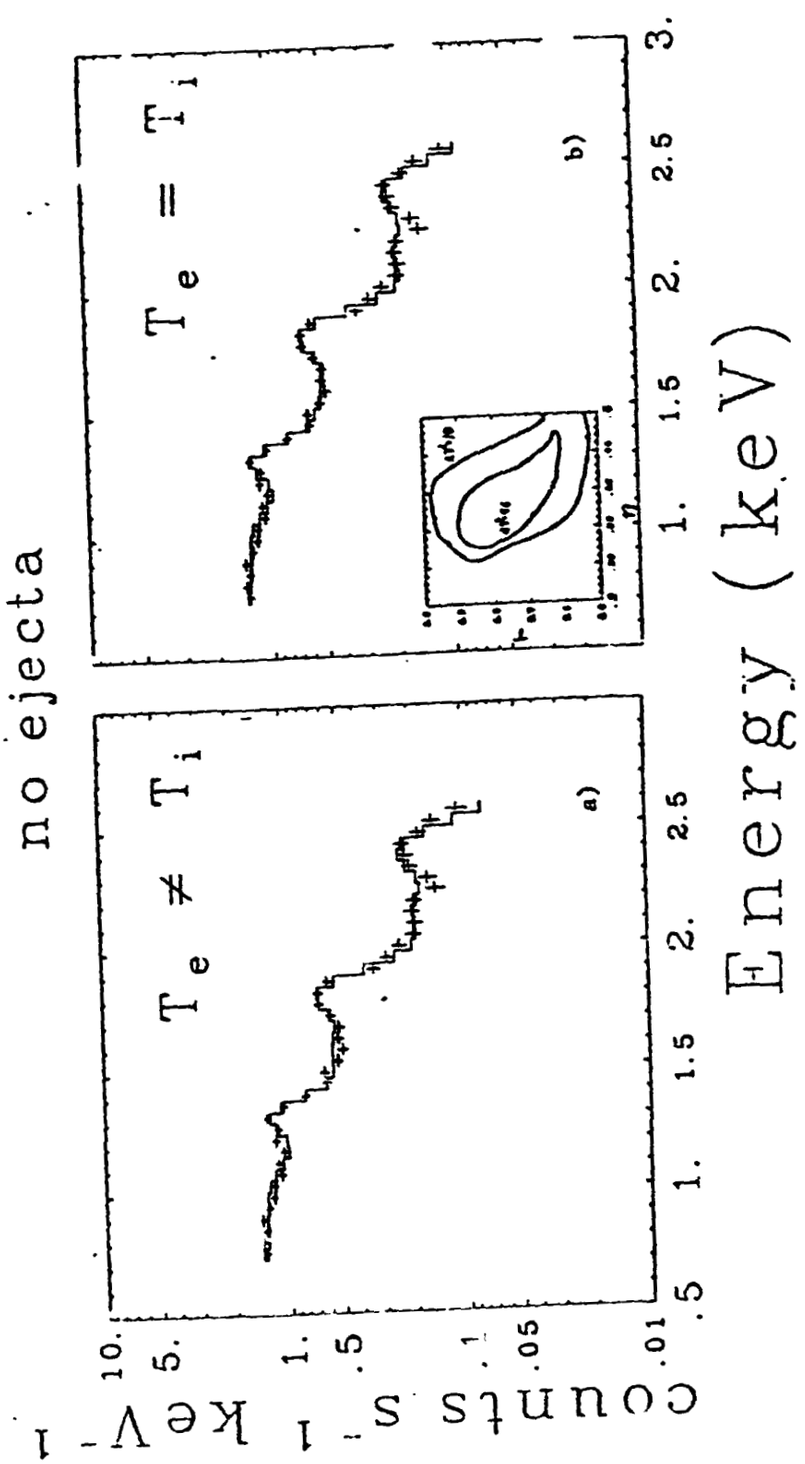

Figure 3

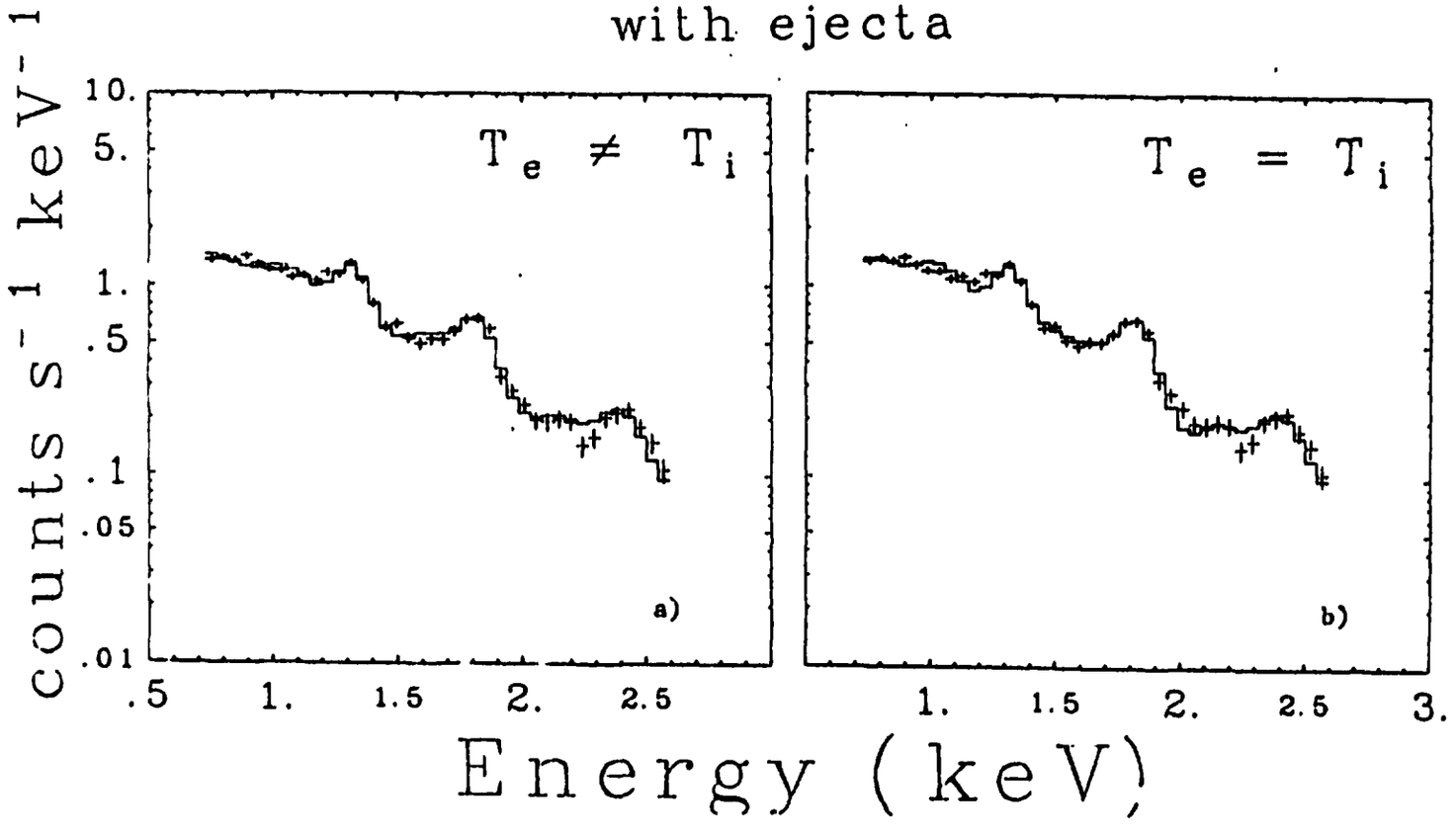

Figure 4

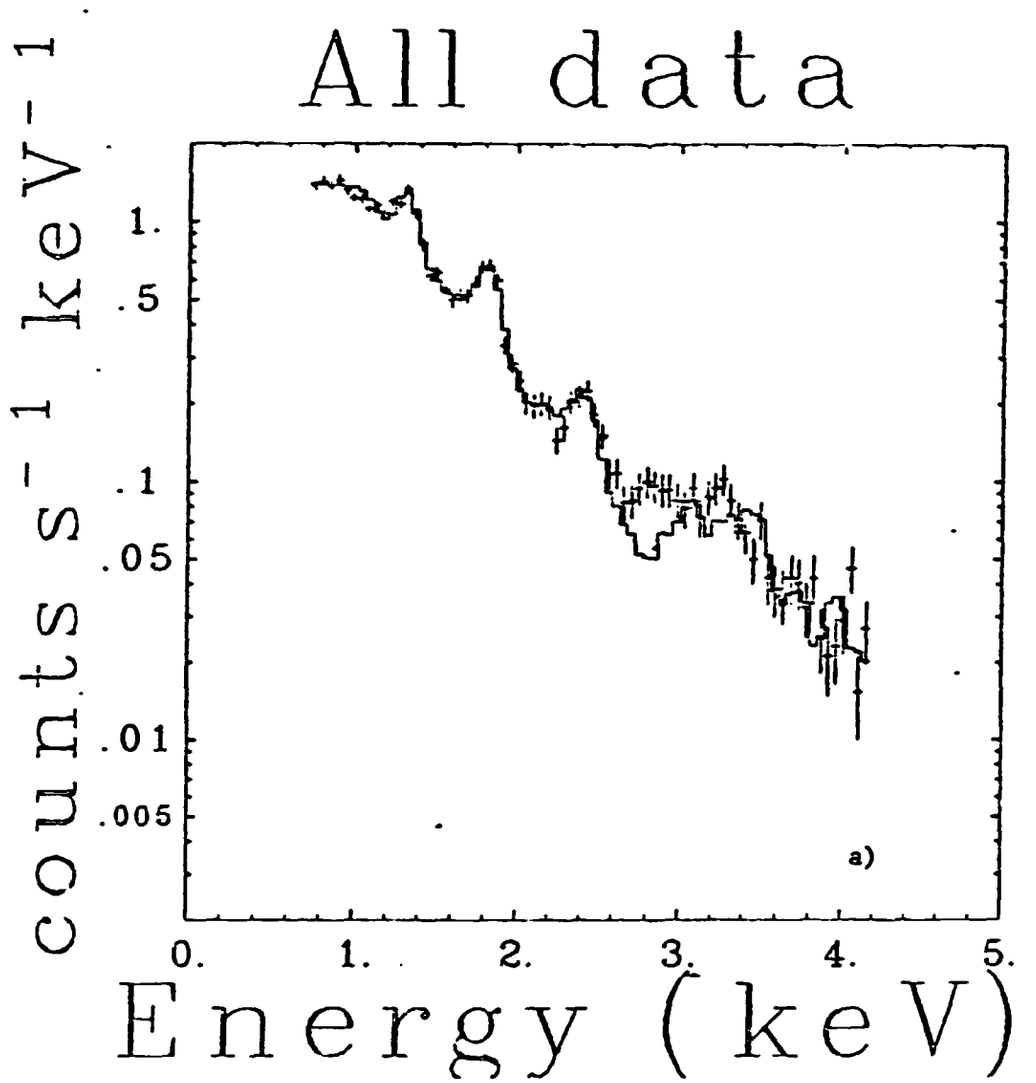

Figure 5

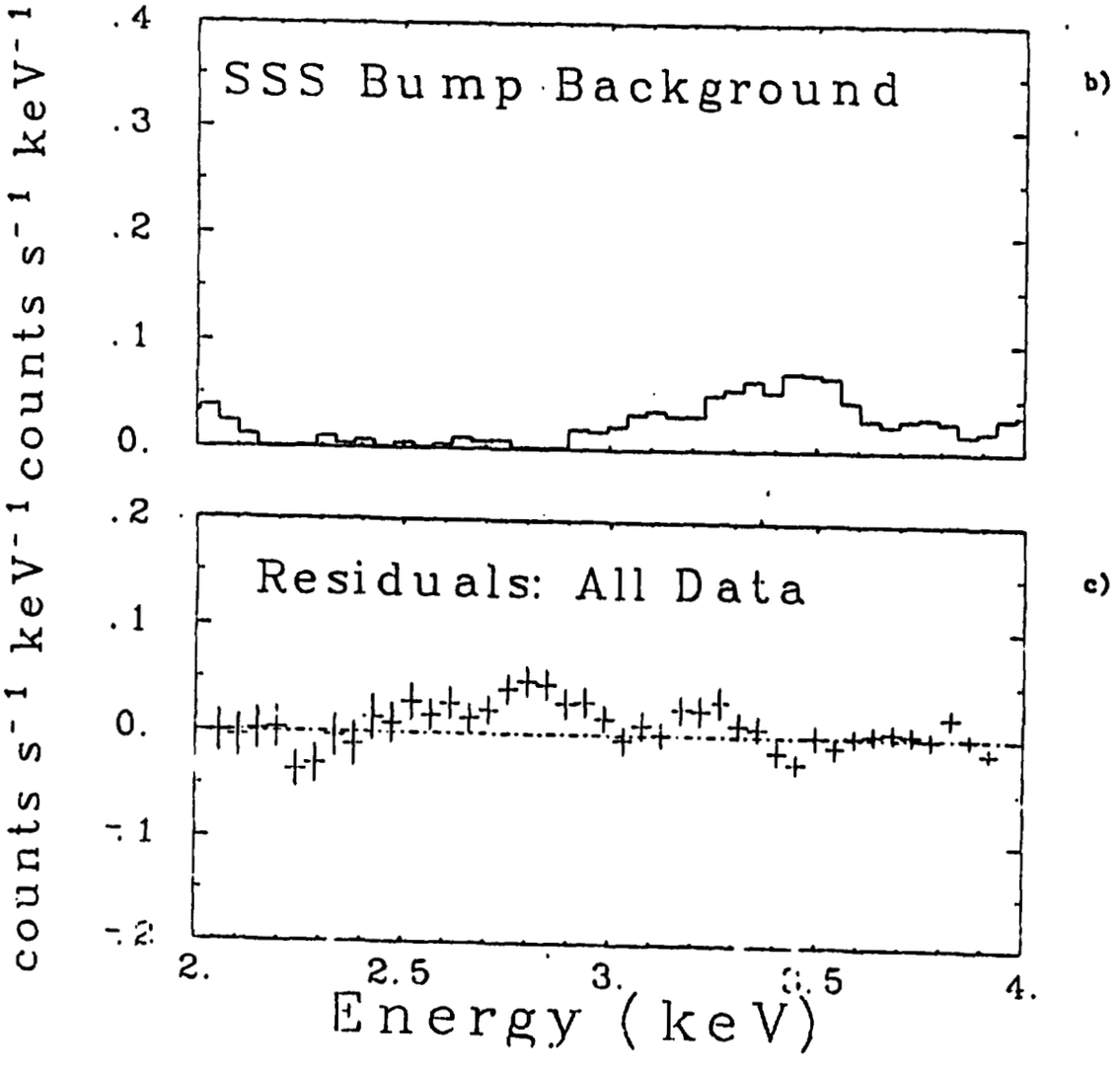

Figure 5 A

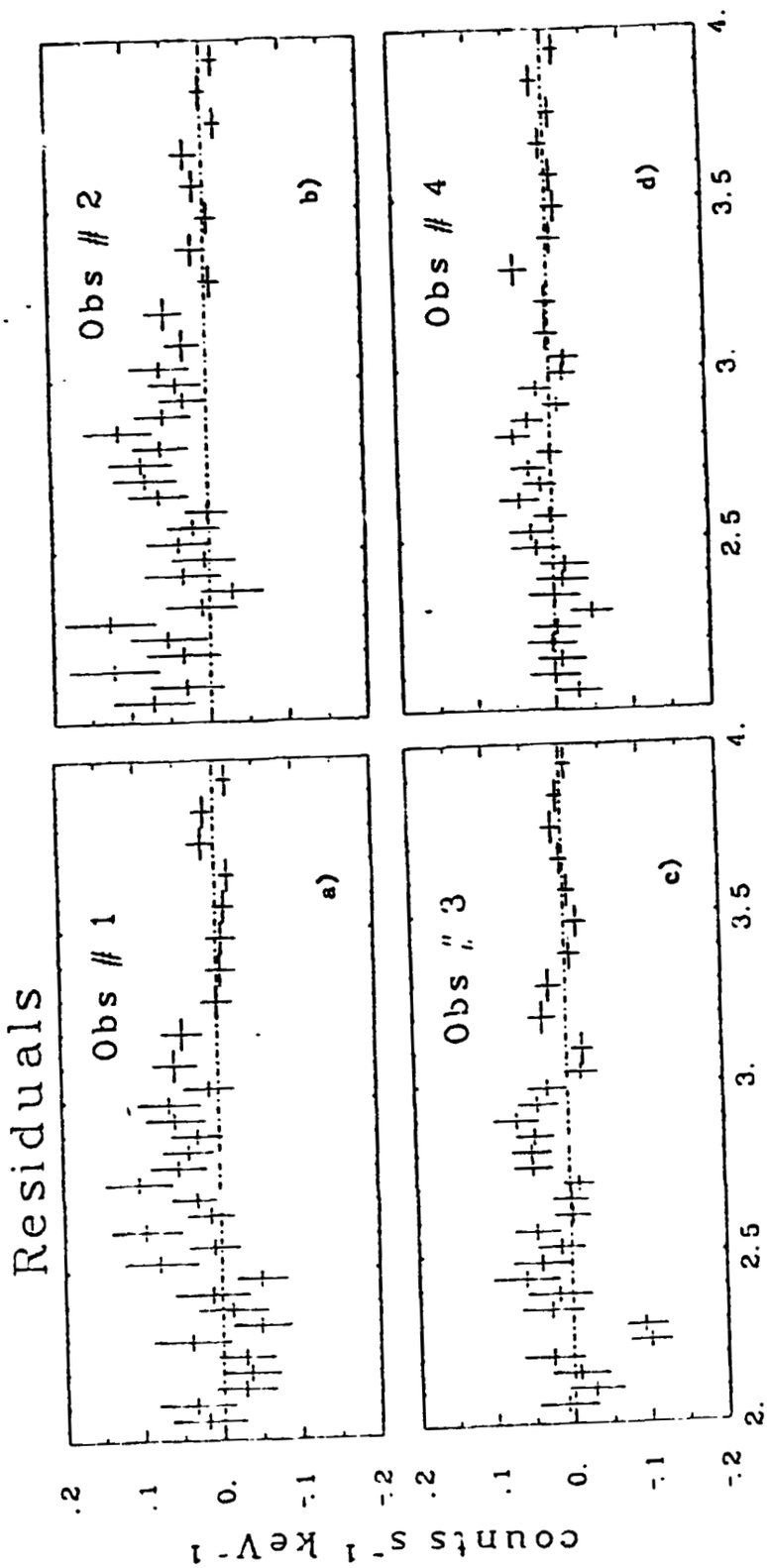

Figure 6

4.4 Concluding Remarks

The NIE models seemed successful from the point of view of the "global" issues since the models did give adequate fits to the data with physically reasonable parameters. The x^2 were somewhat high, but this is reasonable given systematic uncertainties in the modeling of the detectors, known uncertainties in the atomic physics, and deviations at the source from the ideal conditions assumed in the model. Although the existence of these systematic uncertainties gives reason for some caution in accepting inferred remnant parameters, the physically reasonable results do indicate that these models do hold some promise for use in future observations.

CIE model fits to MSH 14-63 data had required two plasmas at different temperatures. The NIE model showed that with the exception of the S and Fe Kα lines, the data could be accounted for by shocked ISM of solar composition. The offending lines only required abundance changes by a factor of $\sim$ 3, but as was discussed they could be explained by the density inhomogenities that do seem to be present in MSH 14-63 or by ejecta.

In the case of the SSS data for RCW 103, CIE modeling again required two temperature components in order to give adequate fits. Abundance anomalies of $\gtrsim$ 2 were required for Mg, Si, S, and Fe to explain the intensity of the line emission. The NIE once more proved successful in providing good fits to the data assuming emission from shocked ISM of near solar composition.

The question of emission from reverse-shocked ejecta was not clearly answered by the work here. For these data sets, β was not a well determined parameter. When β was low, the ejecta was too small an emission component. With increasing β the emission started to become significant but the temperature was so low that the bulk of the flux from the ejecta component was either below the bandpass of the detector or was attenuated by interstellar absorption.

On the issue of electron-ion thermal equilibrium the data from MSH 14-6` resoundingly asserted that some non-Coulomb energy exchange mechanism must exist behind the blast wave. MSH 14-63 joins Cas A and Tycho as young remnants where evidence for a non-Coulomb mechanism have been found. The case of RCW 103 is uncertain. Lack of information in the spectrum above 4 keV makes the interpretation difficult.

Future observations providing simultaneously good spectral and spatial resolution which are planned for the next generation x-ray telescope, can be invaluable for separating the ejecta component of the spectra from the shocked ISM and for establishing whether surface brightness variations within a remnant are due to a filling factors or density inhomogenities. Observations with spectral resolution of $\Delta E/E \lesssim 1\%$ with or without spatial resolution would allow measurement of lines from individual ionic species of the same element. These would allow more direct plasma diagnostics than those in this thesis which had to infer the fine structure from lower resolution spectra.

5.0 Optical Identification of X-ray Sources

Discovery of new X-ray sources is dramatic and can have considerable scientific impact, but until an optical counterpart for the X-ray source is found little further work can be done. This is true because X-ray detectors have comparatively low spatial and spectral resolution, and are encumbered by the necessity of space-borne observatories. Once an optical counterpart is found the full range of accumulated optical experience can be brought to bear, especially in the areas of high resolution spectroscopy and long and short-term variability. An optical position is also precise enough so that instruments in other wavelengths; ultraviolet, infra-red, and radio, for example; can be efficiently utilized.

The specific set of X-ray sources we are concerned with are those discovered by the HEAO-1 A-2 experiment Low Energy Detectors (LED's). This experiment surveyed for the first time over 95% of the sky in the energy band 0.15-2.8 keV down to a limiting magnitude of 1×10^{-11} ergs cm^{-2} s^{-1}. A catalog of the sources seen by this experiment, using a very stringent 6σ existence criteria, contained 114 sources (Nugent et al 1983). To appreciate the impact of this experiment consider that of the 49 sources in this catalog with flux between 0.15 and 0.44 keV only 12 were previously known.

Unfortunately the uncertainty in position of these sources, resulting from the fluctuations in counting statistics was significant. The position was only determined to a characteristic size of $\sim 0.2°$ in one direction and $\sim 3°$ in the other. As the brightest objects in the X-ray sky are not necessarilly bright optically this is far to imprecise to allow optical identification.

To further refine the position it is necessary to acquire more data. We have employed three techniques. In one, the Einstein X-ray Observatory was used to search the HEAO-1 LED error boxes for bright X-ray emitting objects. The Imaging Proportional Counter (IPC) aboard Einstein has a field of view of $\sim 1°$ and

produces X-ray source positions accurate to 1'. An object brighter than twelfth magnitude optically in such a small box was sufficiently uncommon as to make the identification by coincidence. Fainter objects had to be studied spectroscopically to select the X-ray emitter.

The portion of this program partially supported by this grant was the optical identification. Utilizing the Mt. Palomar 60" telescope during the phase at Cal Tech and the Black Moshannon 60" telescope during the phase at Penn State, we performed high and low resolution spectroscopy.

Of eight HEAO-1 source error boxes completely searched by Einstein six produced strong X-ray sources. (The other two are presumably variable and so not detectable during the Einstein observation.) Two of these are located in the Southern Hemisphere and not accessible to Mt. Palomar or Black Moshannon, but we have managed successful cooperation with our southern colleagues (Jensen, Nousek and Nugent 1982; Mason et al 1983; Nousek and Pravdo 1983).

In addition to the bright HEAO-1 sources fainter X-ray sources appear serendipitously in the IPC fields. We have endeavored to identify these as well.

The observing pattern was as follows. For the bright stars, brighter than 12^m, we assumed the star was the X-ray source and undertook high resolution spectroscopy searching for anomalies in the spectrum. For the fainter objects we conducted imaging color photometry to select blue candidates in the field and followed up with low resolution spectroscopy down to $\sim 16^m$. At Mt. Palomar we conducted 18 nights of observing, ten nights to spectroscopy, four nights to imaging photometry and four were clouded out. In this time we performed photometry in three colors on 18 X-ray fields, mostly seredipitous. Low resolution spectral types are obtained for 36 possible candidates, as well as a modest library of comparison spectra. Repeated spectra of 18 bright candidates were obtained at high resolution to look for spectral changes with time.

At Black Moshannon 31 nights were assigned, of which 18 were lost to clouds or equipment failures. The remaining 13 nights were devoted to low resolution spectroscopy of 18 objects, one of which was observed 50 times to follow line profile shifts.

The scientific return of this program has been substantial. A new Seyfert 1 galaxy was discovered at a redshift of Z = 0.038, E1615+061 (Pravdo et al 1981a, Pravdo et al 1981b). The presence of a Seyfert in a catalog of the brightest soft X-ray sources is surprising. The optical properties of E1615+061 seem ordinary (for a Seyfert). Pravdo et al suggest the great soft X-ray luminosity may be typical of Seyferts, but only rarely able to escape the core region of the galaxy. Hence only a few Seyferts at any one time will exhibit the X-ray properties of E1615+061.

The apparently normal ninth magnitude G star HD155638 shows dramatic Ca H and K emission reversals (Nousek et al 1980, Stern et al 1981). These emission reversals are diagnostic of an active chromosphere, which apparently results in a powerful coronal X-ray source. The centroid of the reversal shifts with respect to the absorption profile but the radial velocity of the sharper lines suggest no orbital motion. Either HD155638 is a binary system of two extremely similar stars, in which only one is active, or it is a single star rotating rapidly with highly confined surface regions of activity. While HD155638 shows some similarity to the RS Canes Venaticorum stars, the most active coronal emitters, there are still some differences.

A very recent discovery has been a new AM Herculis type binary system E2003+225 (Nousek et al 1982, Nousek et al 1983). These systems consist of a low mass star orbiting around a highly magnetized white dwarf. Rather than the accretion disk found in most astrophysical accretion situations in AM Her stars the strong magnetic field channels the flow into an accretion columns. The study of these systems is particularly intriguing because of the complex behavior

of the emission line profiles and doppler shifts, strong and variable optical polarization and high UV and X-ray luminosity and variability. Of about a dozen AM Her systems known E2003+225 has the longest period (3^h 42^m) and thus both makes observations easier and probes the effect of system separation on the phenomena of the type. A paper combining HEAO-1, Einstein, high speed photometry and circular and linear polarization is currently in preparation.

A similar systems with weaker magnetic fields, AC Cancri, is a strong candidate for another HEAO-1 source. Time resolved spectroscopic observation of AC Cnc through eclipse with the Palomar 200" telescope are currently being reduced.

Useful as this technique is, the demise of the Einstein Observatory has forced us to look for alternative means of identifying the remaining 36 sources. Of the HEAO-1 sources located by Einstein nearly all were typified by emission line spectra, and all are relatively bright ($\lesssim 15^m$). Optical techniques to search for emission line and blue continuum objects exist. One of the best is to use a wide field Schmidt telescope with an objective prism. We have taken at series of 22 plates in this way, using the 24" Burrell Schmidt at Kitt Peak National Observatory and the 24" Curtiss Schmidt at the Cerro Tololo Inter-American Observatory. With a single exposure the Schmidt telescopes take low resolution spectra of every object within the 5° x 5° field of view. This is easily large enough to include the entire HEAO-1 error box. The major problem lies in the analysis of the plates. At galactic latitudes below 20° the confusion of spectra prohibits the use of this technique.

The plates taken in these two runs (April and November, 1982) have been searched and seven promising candiates resulted. Higher resolution spectroscopic work and IUE observations are underway to better identify these objects.

The third optical technique we are using to study X-ray souces is to search for rapid variability. Jensen (1982) has used the HEAO-1 LED data to contrain

the X-ray emitting properties of the old nova and nova like variable sub-class of cataclysmic variable. Current theory suggests these variables are only in outburst infrequently, but the observed number of outbursts is relatively high. If this is true then many of these variables are near us 'waiting' to go into outburst. Their X-ray emission should be statistically detected as a population of moderately bright X-ray source.

Jensen (1982) finds there are too few such sources to resolve the missing dwarf nova problem and concludes the X-ray emission must be smothered. If this is true then the old novae can only be detected by their rapid optical variability.

In order to search for variable stars, short ($\sim 15^m$) exposures using the Palomar 48" Schmidt telescope have been taken of the same 7° x 7° part of the sky. A series of nine such plates, containing 27 images, have been collected. Most stars will produce 27 approximately equal images, but stars which vary over short timescales will produce varying images.

The major difficulty in this program is selecting out the varying images from the $\sim 10^5$ star images on each plate. The Image Processing Lab at the Jet Propulsion Lab has kindly offered to digitize and analyse a trial plate. This computer selection process is not perfect, but from the top 50 candidates picked by the computer we have found evidence of variability in six on timescales of 30 minutes or less. Follow up spectroscopic studies will be undertaken at Black Moshannon Observatory this summer.

6.0 Evaluation of certain Metal Oxides as X-ray Detectors

Current X-ray detectors possess energy resolution which is determined by the fluctuation in the number of ion-electron pairs generated in the detector following photoelectric absorption of an X-ray. For gaseous detectors the energy required to produce an ion-electron pair is of the order of 25 eV. The fluctuations in the signal generated by a mean number of ion-electron pairs is proportional to the square root of this number for a given material times a factor (Fano factor) which modifies this statistical process based on the production of ion-electron pairs by the photo electron. Counter effects, such as variable gas gain and charge collection, are sometimes lumped with this correction to provide an overall correction to the statistical fluctuations in the mean charge generated in the interaction.

Solid state detectors based on Si, Ge or HgI_2 require less energy to generate an ion-electron pair than a gas, since the valence and conduction electrons require less energy to remove them from the nuclear charge when the atoms are bound in a solid. The energy for these solids are roughly 4 eV to generate an ion-electron pair.

Transition metal oxides are thought to require less energy to produce an ion-electron pair than other solids because of the nature of d-electrons forming the bonds in the crystal lattice. The energies may be as low as one eV or slightly more. If such a material can be found for which electron trapping is not high, then a factor of up to two in intrinsic energy resolution could be achieved. No direct measurements of this quantity has been made on transition metal oxides, so a program was initiated to obtain some basic data on several such materials including V_2O_5, Cr_2O_3, TiO_2 and MnO, all of which show electrical properties at low temperature which can yield data on the ion-electron pair production and electron trapping.

A crystal of each of the above substances has been obtained. A laboratory set up has been developed for coating the crystals with gold to provide electrical

contact. A dewar for cooling and a thermistor thermometer has been constructed for the measurements. Unfortunately, the graduate student working on this problem decided to go into theory, so the measurements have not been completed at this time. They will be carried out by a lab assistant in the next few months.

Allen, C. W., 1976, Astrophysical Quantities, 4th ed. (London; The Athlone Press).

Bachall, J. N., and Wolf, R. A. 1965, Ap.J., 142, 1254.

Becker, R. H., Holt, S. S., Smith, B. W., White, N. E., Boldt, E. A., Muchotzky, R. F. and Serlemitos, P. J. 1980, Ap.J. (Letters), 235, L5.

Bevington, P. R. 1969, Data Reduction and Error Analysis for the Physical Sciences (New York; McGraw-Hill).

Caswell, J. L., Clark, D. H., and Crawford, D. F. 1975, Australian J. Phys. Suppl., 37, 39.

Caswell, J. L. et al. 1976, Astron. Astrophys.

Chevalier, R. A., 1977, Ann. Rev. Astr. Ap., 15, 175.

Chevalier, R. A. 1975, Ap.J., 200, 698.

Clark, D. H. and Caswell, J. L. 1976, M.N.R.A.S., 174, 267.

Clark, D. H. and Stephenson, F. R., 1977, Historical Supernovae (Oxford; Pergamon Press).

Cox, D. P. and Anderson, P. R. 1982, Ap.J., 253, 268.

Fireman, E. L. 1974, Ap.J., 187, 57.

Glen, G. and Sutherland, P. G. 1980, Ap.J., 239, 671.

Groenshild, E. H. B. M., 1979 Utrecht University Ph.D. thesis.

Goss, W. M., and Shaver, P. A. 1970, Aust. J. Phys., Astro. Suppl., 14, 1.

Gull, S. F. 1973, M.N.R.A.S., 161, 47.

Gull, S. F. 1975, M.N.R.A.S., 171, 263.

Hamilton, A. J. S., Sarazin, C. L., and Chevalier, R. A. 1982 (preprint).

Hill, E. R. 1967, Australian J. Phys., 20, 297.

Itoh, H., 1977, Publ. Astr. Soc. Japan, 29, 813.

Itoh, H., 1978, Publ. Astr. Soc. Japan, 30, 489.

Itoh, H., 1979, Publ. Astr. Soc. Japan, 31, 541.

Jensen, K. A., 1982, Ph.D. Thesis, California Institute of Technology.

Jensen, K. A., Nousek, J. A., and Nugent, J. J., "H1409-45: A Recurrent Soft X-ray Transient", Ap.J., 261, 625, 1982.

Joyce, R. M., Becker, R. H., Birsa, F. B., Holt, S. S., and Noordzy, M. P. 1978, IEEE Trans. Nucl. Sci., 25, 453.

Kato, T. 1976, Ap.J. Suppl., 30, 397.

Lampton, M. et al. 1976, Ap.J., 208, 177.

Lucke, R. L., et al. 1979, Ap.J., 228, 763.

Mansfield, V. N., and Salpeter, E. E. 1974, Ap.J., 190, 305.

McKee, C. F. 1974, Ap.J., 188, 335.

Mewe, R., Schrijver, J., and Sylwester, J., 1980, Astr. Ap. Suppl., 40, 323.

Meyer, J., 1979, Les Elememts et leurs Iostope dans l'Univers, Comm. 22nd Colloq. Int. d'Astrophys. Liese, p. 153.

Moore, W. C. and Garmire, G. P., 1976, Ap.J., 206, p. 247.

Naranan, S. et al. 1977, Ap.J. (Letters), 213, L53.

Normoto, K. and Tsurta, S. 1981, Ap.J. (Letters), 250, L19.

Nousek, J. A. and Pravdo, S. H., "IUE Observations of E1405-451: A New AM Her-type Cataclysmic Variable", Ap.J. (Letters), 266, L39, 1983.

Nugent, J. J. and Garmire, G. P. 1978, Ap.J. (Letters), 226, L83.

Nugent, J. J. et al. 1982, Ap.J. Suppl., (accepted).

Nugent, J. J., Jensen, K., Nousek, J. A., Garmire, G. P., Mason, K., Walter, F., Bowyer, S., Stern, R., and Riegler, G. R., "HEAO-A2 Soft X-ray Source Catalog", Ap.J. Suppl., 51, 1, 1983.

Nussbaumer, H. and Osterbrook, D. E. 1970, Ap.J., 161, 811.

Pradhan, A. K., Norcross, D. W., and Hummer, D. G. 1981, Ap.J., 246, 1031.

Pravdo, S. H. and Smith, B. W. 1979, Ap.J. (Letters), 234, L195.

Pravdo, S. H., Nugent, J. J., Nousek, J. A., Jensen, K., Wilson, A. S., and Becker, R. H., "Discovery of a Seyfert 1 with an Unusually Soft X-ray Spectrum", Ap.J., 251, 501, 1981.

Raymond, J. C. and Smith, B. W. 1977, Ap.J. Suppl., 35, 419.

Richardson, M. B., et al. 1982, Ap.J., 255, 624.

Richtmyer, R. D., and Morton, K. W., 1967, Difference Methods for Initial-Value Problems, 2nd ed. (New York; InterScience).

Riegler, G. R., Stern, R. A., Liewer, K., Vescelus, F., Nousek, J. A. and Garmire, G. P. 1981, NASA Technical Memorandum #83848, "X-ray Astronomy in the 1980's", p. 289.

Rothschild, R. et al., 1979, Space Sci. Inst., 4, 169.

Sedov, L., 1959, Similarity and Dimensional Methods in Mechanics, (New York; Academic).

Shlovsky, I. S., 1962, Soviet Asto., 6, 162.

Shull, J. M. 1981, Ap.J. Suppl., 46, 27.

Shull, J. M., 1982, (preprint).

Solinger, A., Rappaport, S., and Buff, J. 1975, Ap.J., 201, 381.

Spitzer, L. 1962, Physics of Fully Ionized Gases, 2nd ed., (New York; InterScience).

Spitzer, L. 1978, Physical Process in the Interstellar Medium, (New York; Inter-Science).

Stern, R. A., Liewer, K., and Janesick, J. R., 1983, R.S.I. 54(2), 196.

Stern, R. A., Nousek, J. A., Nugent, J. J., Agrawal, P. C., Riegler, G. R., Rosenthal, A. J., Pravdo, S. H., and Garmire, G. P., "X-ray and Optical Observations of HD155638: A Remarkably Active Cool Star", Ap.J. (Letters), 251, L105, 1981.

Tuohy, I. R. et al. 1979, Ap.J. (Letters), 230, L27.

Tuohy, I. R. and Garmire, G. P. 1980, Ap.J. (Letters),

Tuohy, I. R. et al., 1983 (in preparation).

Tucker, W. H., and Koren, M. 1971, Ap.J., 168, 283.

Westerlund, B. E. 1969a, Astron. J., 74, 879.

Westerlund, B. E. 1969b, Astron. J., 74, 882.

Winkler, P. F. 1978, Ap.J., 221, 220.

Winkler, P. F., Canizares, C. R., Clark, G. W., Market, T. H., and Petre, R., 1981, Ap.J., 245, 574.

Papers and Abstracts supported by the Grant

S. Pravdo, J. Nugent, J. Nousek, K. Jensen, A. Wilson, and R. Becker, 1981 BAAS, 13, 521.

J. Nousek, R. Stern, J. Nugent, A. Rosenthal, S. Pravdo and G. Garmire 1980, BAAS, 12, 855.

"X-ray and Optical Observations of HD155638: A Remarkably Active Cool Star", R. A. Stern, J. A. Nousek, J. J. Nugent, P. C. Agrawal, G. R. Riegler, A. J. Rosenthal, S. H. Pravdo, and G. P. Garmire, Ap.J. (Letters), 251, L105, 1981.

"Discovery of a Seyfert 1 with an Unusually Soft X-ray Spectrum" S. H. Pravdo, J. J. Nugent, J. A. Nousek, K. Jensen, A. S. Wilson, and R. H. Becker, Ap.J. 251, 501, 1981.

J. Nousek, G. Luppino and S. Gajar, 1982 IAU Circular No. 3733.

J. Nousek, L. Takalo, H. Bond, G. Schmidt, and S. Tapia, 1982, BAAS, 14, 980.

G. R. Riegler, R. A. Stern, K. Liewer, F. Vescelus, J. A. Nousek and G. P. Garmire 1981, NASA Technical Memorandum #83848, "X-ray Astronomy in the 1980's", p. 289.